

## Neutrino flavor ratios as diagnostic of solar WIMP annihilation

Ralf Lehnert<sup>1,2,\*</sup> and Thomas J. Weiler<sup>3,†</sup><sup>1</sup>*Center for Theoretical Physics, Massachusetts Institute of Technology, Cambridge, MA 02139, USA*<sup>2</sup>*Max-Planck-Institut für Physik, Föhringer Ring 6, 80805 München, Germany*<sup>3</sup>*Department of Physics and Astronomy, Vanderbilt University, Nashville, TN 37235, USA*

(Dated: October 27, 2018)

We consider the neutrino (and antineutrino) flavors arriving at Earth for neutrinos produced in the annihilation of weakly interacting massive particles (WIMPs) in the Sun's core. Solar-matter effects on the flavor propagation of the resulting  $\gtrsim$  GeV neutrinos are studied analytically within a density-matrix formalism. Matter effects, including mass-state level-crossings, influence the flavor fluxes considerably. The exposition herein is somewhat pedagogical, in that it starts with adiabatic evolution of single flavors from the Sun's center, with  $\theta_{13}$  set to zero, and progresses to fully realistic processing of the flavor ratios expected in WIMP decay, from the Sun's core to the Earth. In the fully realistic calculation, non-adiabatic level-crossing is included, as are possible nonzero values for  $\theta_{13}$  and the CP-violating phase  $\delta$ . Due to resonance enhancement in matter, nonzero values of  $\theta_{13}$  even smaller than a degree can noticeably affect flavor propagation. Both normal and inverted neutrino-mass hierarchies are considered. Our main conclusion is that measuring flavor ratios (in addition to energy spectra) of  $\gtrsim$  GeV solar neutrinos can provide discrimination between WIMP models. In particular, we demonstrate the flavor differences at Earth for neutrinos from the two main classes of WIMP final states, namely  $W^+W^-$  and 95%  $b\bar{b} + 5\% \tau^+\tau^-$ . Conversely, if WIMP properties were to be learned from production in future accelerators, then the flavor ratios of  $\gtrsim$  GeV solar neutrinos might be useful for inferring  $\theta_{13}$  and the mass hierarchy. From the full calculations, we find (and prove) some general features: a flavor-democratic flux produced at the Sun's core arrives at earth still flavor-democratic; for maximal  $\theta_{32}$  but arbitrary  $\theta_{21}$  and  $\theta_{13}$ , the replacement  $\delta \rightarrow \pi - \delta$  leaves the  $e$  flavor spectra unaltered but interchanges  $\mu$  and  $\tau$  spectra at Earth; and, only for neutrinos in the inverted hierarchy and antineutrinos in the normal hierarchy is the dependence on the mixing phase  $\delta$  not suppressed to order  $\delta m_{21}^2/\delta m_{32}^2$ .

PACS numbers: 14.60.Pq, 95.85.Ry, 26.65.+t, 95.35.+d

## I. INTRODUCTION

One of the most fundamental questions about our Universe is its matter content. Recent cosmological observations of type Ia supernovae [1], the cosmic microwave background [2], galaxy-cluster evolution [3], and gravitational lensing [4] show that known particle species contribute only  $\Omega_B \simeq 4\%$  to the total energy density of the Cosmos. Abundance measurements of light elements together with the theory of Big-Bang Nucleosynthesis largely support these findings [5]. The above results also indicate the presence of two—as yet unknown—matter components: “dark energy” and “dark matter” with relative densities of  $\Omega_{DE} \simeq 73\%$  and  $\Omega_{DM} \simeq 23\%$ , respectively. Unraveling the nature of these novel types of matter lies currently on the forefront of fundamental-physics research.

One of the new components, dark matter (DM), exhibits gravitational clustering and is therefore believed to be composed of novel massive particles. Further compelling support for this idea is provided by theoretical approaches to physics beyond the Standard Model, which typically require additional particles for consis-

tency. Weakly interacting massive particles (WIMPs) are a general and popular candidate in this context. A particularly attractive example of a WIMP is the lightest supersymmetric particle (LSP), usually the neutralino, present in various SUSY extensions of the Standard Model [6]. This particle is a mixture of the four superpartners of the two neutral Higgs particles and the two neutral electroweak gauge bosons. The neutralino is expected to have a mass of order  $10^2$  GeV. The attractiveness of identifying the LSP with dark matter is twofold: First, the LSP is stable, assuming  $R$ -parity is an unbroken symmetry.  $R$ -parity is introduced to stabilize the proton to the level required by experiment. Second, a standard thermodynamic calculation of decoupling yields the LSP abundance to be  $\mathcal{O}(10^{-34} \text{cm}^2/\sigma_A)$ , where  $\sigma_A$  is the WIMP annihilation cross section for Majorana particles like the neutralino (for Dirac WIMPs, there is an additional factor of  $T_{\text{decouple}}/M_{\text{WIMP}} \sim 1/30$ ). Inputting the usual weak cross section  $\sigma_A(s = M_{\text{WIMP}}^2) \sim G_F^2/\pi$ , one naturally explains the inferred value  $\Omega_{DM} \simeq 23\%$  [7, 8].

Besides direct detection via WIMP scattering in cryogenic detectors, indirect searches for WIMP annihilation into gamma rays, antimatter, and neutrinos are currently being pursued as promising experimental avenues [9, 10]. The gravitational fields of the Sun and the Earth can capture large numbers of WIMPs, which are expected to then infall toward the center of the body [11]. Since the annihilation rate is proportional to  $n_{DM}^2$ , annihila-

\*Electronic mail: rlehnert@lns.mit.edu

†Electronic mail: tom.weiler@vanderbilt.edu

tions of WIMPs captured by the Sun or Earth may be considerable. An important factor in WIMP capture is the surface area of the capturing body. Another is the efficiency of capture  $\epsilon_{\text{cptr}}$ , which is related to the depth of the potential well relative to the mean kinetic energy of the infalling WIMP. The capture rate is proportional to the square of the body area and to the capture efficiency. There results a relative Sun-to-Earth capture rate of  $(\epsilon_{\text{cptr}}^{\text{Sun}}/\epsilon_{\text{cptr}}^{\text{Earth}})(R_{\odot}/R_{\oplus})^2$ , where  $R_{\odot} = 6.96 \times 10^{10}$  cm is the radius of the Sun and  $R_{\oplus} = 6.38 \times 10^8$  cm the radius of the Earth. Allowing for the  $1/D^2$  flux dilution between the source and the earthly detector, one then arrives at a naïve relative flux ratio at Earth of  $F_{\text{Sun}}/F_{\text{Earth}} \sim (\epsilon_{\text{cptr}}^{\text{Sun}}/\epsilon_{\text{cptr}}^{\text{Earth}})(R_{\odot}/R_{\oplus})^2(R_{\oplus}/\text{AU})^2 = 2 \times 10^{-5}(\epsilon_{\text{cptr}}^{\text{Sun}}/\epsilon_{\text{cptr}}^{\text{Earth}})$ . Three further pieces of physics more than compensate the  $10^{-5}$  factor and make the Sun the better source for experimental study. First, the capture efficiency of the Sun far exceeds that of the Earth, with relative potentials  $\sim M/R$  that are 3000 times larger for the Sun. The second is that the solar potential reduces the lifetime of WIMP orbits among the planets, thereby reducing the capture rate at Earth [7]. The third factor is that center-pointing gravitational force  $\sim M(< r)/r^2$  is far greater for the Sun, due to its roughly exponential relation between density and radius. In fact, the DM in the Earth is not concentrated in Earth’s center but rather broadly distributed in  $r$ . As a consequence,  $n_{\text{DM}}^2$  is not optimized in the Earth, and the annihilation signal is fairly diffuse because it comes from a large fraction of a steradian. On the other hand, the Sun has a high central DM density, and an annihilation signal coming from a fraction of a square degree of solid angle. Thus, we will not consider further the WIMP annihilation flux coming from the Earth, but rather focus on the annihilation signal from the Sun.

The solar medium absorbs all annihilation products except neutrinos with energies below tens of GeV. The typical energies of fusion neutrinos are 10 MeV or less, while the typical energies of neutrinos and antineutrinos from the WIMP decay chain are GeV to tens of GeV. It follows then that the detection of higher-energy neutrinos from the Sun provides an excellent tool for indirect WIMP detection.

The idea of inferring WIMPs by measuring the associated high-energy neutrino flux from the Sun’s center has been the focus of numerous theoretical studies [12], and first experimental results have placed loose constraints on such scenarios [13]. Note, however, that neutrino detection is highly dependent on neutrino flavor ( $\nu_e$  versus  $\nu_{\mu}$  versus  $\nu_{\tau}$ ). These flavors evolve as the neutrinos travel in space and time. This is particularly so in the Sun, where the solar environment adds significant matter-dependent effects to the flavor evolution [14]. In fact, matter effects do not only alter the flavor evolution, but they also treat the neutrino and antineutrino differently. Therefore, dark-matter searches via annihilation neutrinos typically require considerable knowledge of neutrino mixing and mass parameters.

Matter effects were not included in the early works cited in [12]. More recently, the MSW effect has been incorporated into the analysis of solar WIMP annihilation neutrinos by a number of authors [15–18]. Of these, only [18] is recent enough to have focused on the “last-solar-model-standing,” the large mixing angle (LMA) solution. The other papers hedged their bets among LMA, SMA, LOW, and VAC solutions appropriate for their time when less was known [19].

Although our knowledge of neutrino parameters has advanced quickly, it remains incomplete. The neutrino mixing angles seem to converge to a “tribimaximal” form [20] with values in vacuum given to a good approximation by  $\sin^2 \theta_{23} \sim 1/2$ ,  $\sin^2 \theta_{12} \sim 1/3$ , and  $\sin^2 \theta_{13} \sim 0$ . The large value of the “solar” angle  $\theta_{12}$  lies at the heart of the LMA solution. The neutrino mass-squared differences have converged to  $\delta m_{23}^2 \sim 2.5 \times 10^{-3} \text{eV}^2$  and  $\delta m_{12}^2 \sim 0.8 \times 10^{-4} \text{eV}^2$ .

In Ref. [18], numerically precise terrestrial spectra resulting from the primary WIMP-annihilation channels are predicted, signal topologies in neutrino telescopes are given, and the possibility of discriminating among dark-matter models is discussed. Our investigation complements that in Ref. [18] mainly in two ways.

First, we focus on particularly promising observables: there has been a growing awareness in recent years that neutrino telescopes can infer *flavor ratios* of arriving neutrinos. It has been shown [21] that neutrino flavor ratios may be determined in ice and water neutrino telescopes from the observation of the ratio of muon-track events to jet events, where the former arise from charged-current (CC)  $\nu_{\mu}$  scattering, and the latter from  $\nu_e$  and  $\nu_{\tau}$  CC events and all neutral-current (NC) events. The muon mean-free-path (MFP) before decay is  $c\tau_{\mu} \sim 6.3 \text{ km } (E_{\mu}/\text{GeV})$ , which allows even 100 MeV muons to be identified. Large-volume magnetized-iron calorimeters, liquid-Argon detectors, and active-scintillator detectors have the potential to perform even better neutrino-flavor identification [22]. The  $\tau$  MFP is  $c\tau_{\tau} \sim 0.49 \times 10^{-2} \text{ cm } (E_{\tau}/\text{GeV})$ , leading to possibly identifiable  $\tau$  tracks for energies above 10 GeV.

Second, we use a related but different treatment of the propagation of  $E \gtrsim \text{GeV}$  neutrinos from the solar core to Earth. We employ a density-matrix formalism and arrive at compact and convenient analytic results which we believe improve our intuition.

Besides presenting matter effects that alter the flavor content of a propagating neutrino flux, possibly resonantly, solar matter also absorbs neutrinos above some energy  $E_{\text{abs}}$ , due to the neutrino inelastic CC and NC interactions. We wish to neglect absorption by looking at neutrinos with  $E < E_{\text{abs}}$ . So we must estimate  $E_{\text{abs}}$ . In the Sun, the number density of electrons  $n_e$  decreases nearly exponentially with the distance  $r$  from the Sun’s center. An approximate expression for the solar density profile  $n_e(r)$  is given by [23]

$$n_e(r) = 245 N_A e^{-r/\lambda_{\odot}} \text{ cm}^{-3}, \quad \lambda_{\odot} = 0.095 R_{\odot}, \quad (1)$$

for  $r \leq R_\odot$ ;  $N_A$  is Avogadro's number. Equation (1) also serves as a rough estimate of the proton and neutron densities.

Integration of this expression from  $r = 0$  to  $r = R_\odot$  gives the column density  $S_j$  from the Sun's center to its surface:

$$S_e = S_p \simeq S_n \simeq 1.6 N_A \times 10^{12} \text{ cm}^{-2}. \quad (2)$$

(For  $R_\odot \gg \lambda_\odot$ , one also has  $S_j \simeq n_j(0) \lambda_\odot$ .) The neutrino's optical depth  $\tau_\nu$  is the number of scattering MFPs from the Sun's center to the surface (the most probable number of interactions in transit); the fraction of produced neutrinos that escape the Sun is  $e^{-\tau_\nu}$ . The optical depth is equal to the product of cross section  $\sigma_\nu$  and column density. Since  $\sigma_{\nu N} \gg \sigma_{\nu e}$  and  $S_p + S_n \simeq 2 S_e$ , we have for the optical depth  $\tau_\nu \sim 2 \sigma_{\nu N} S_e$ . If we ask that a fraction  $f$  or more of the neutrino flux escapes from the Sun, we require

$$\tau_\nu \leq \ln f^{-1}. \quad (3)$$

With the onset of deep inelastic scattering at  $\sim$  GeV energies, the neutrino and antineutrino cross sections grow linearly with  $E$  until  $W$ -propagator effects become important near  $E \sim M_W^2/2m_N \sim$  TeV. To a good approximation, the expression for the inelastic CC+NC neutrino and antineutrino cross sections at energies between 1 GeV and 1 TeV is [24]:

$$\sigma_{\nu N}(E) \simeq 2 \sigma_{\bar{\nu} N}(E) \simeq \frac{E}{\text{GeV}} 10^{-38} \text{ cm}^2. \quad (4)$$

The rules of thumb are that the neutrino cross section is twice the antineutrino cross-section, and the CC contribution is a bit over twice the NC contribution. Also, the fractional energy loss per scatter is about 1/2 for neutrinos at the energies relevant here, and half that again for antineutrinos. In CC scattering, the neutrinos and antineutrinos are lost upon the first scatter; in NC scattering, the neutrinos and antineutrinos persevere but with the fractional energy losses just presented. Since the NC/CC scattering ratio is less than a half, we may and will neglect NC scattering in what follows.

The energy  $E_{\text{abs}}$  can now be calculated by substituting Eq. (4) and twice times Eq. (2) for  $\tau_\nu$  in Eq. (3). The result is  $E_{\text{abs}} = 50 (\ln f^{-1}) \text{ GeV}$  for neutrinos, and twice that for antineutrinos. Some explicit numerical results for  $E_{\text{abs}}^\nu = 2 E_{\text{abs}}^{\bar{\nu}}$  are 10 GeV when  $f = 90\%$ , 36 GeV when  $f = 70\%$ , and 70 GeV when  $f = 50\%$ . If we discount the NC processing of neutrinos and attribute absorption to only the CC, then  $E_{\text{abs}}$  is 50% larger. A careful numerical calculation of absorption versus energy is given in Fig. 1 of Cirelli *et al.* [18]. The conclusion there and here is that up to energies of  $\sim 10$  GeV, absorption in the Sun can be neglected, and above 100 GeV absorption is severe.

The format of this paper is as follows. Flavor oscillations are presented in Sec. II. Matter effects, both adiabatic and non-adiabatic, the two possible mass hierarchies, and zero versus nonzero  $\theta_{13}$  and  $\delta$  are discussed in

detail. In particular, two interesting theorems for the  $\delta$  dependence of the neutrino flavors, valid for the adiabatic regime, are presented. The application of the formalism to the solar WIMP annihilation is made in Sec. III. A summary and conclusions comprise Sec. IV. Some technical details are collected in four appendices.

## II. PHYSICS OF FLAVOR MIXING

This section presents a density-matrix approach for the flavor evolution of high-energy neutrinos injected at the center of the Sun. In the first two subsections, certain simplifying assumptions regarding neutrino-mixing parameters and neutrino propagation in matter are employed; our goal is to set up our formalism and notation, to provide intuition about the involved effects, and to set the stage for a more sophisticated study in the third subsection.

### A. Review: oscillations without matter

In the absence of a matter background (i.e., in vacuum), the free-neutrino Hamiltonian is diagonal in the mass basis:

$$H_M = E \mathbf{1} + \frac{1}{2E} \text{diag}(m_1^2, m_2^2, m_3^2) + \mathcal{O}(m^4/E^3). \quad (5)$$

Here,  $E$  is the neutrino's energy, and  $\mathbf{1}$  is the  $3 \times 3$  unit matrix. We label the mass eigenvectors in vacuum as  $|j\rangle = |1\rangle, |2\rangle, |3\rangle$ . However, neutrinos are produced by the weak interaction. In this production basis, called the "weak basis" or "flavor basis," the interaction eigenstates are labeled by the flavors of their charged-current partners, as  $|\alpha\rangle = |e\rangle, |\mu\rangle, |\tau\rangle$ . In general, the flavor basis is rotated with respect to the mass basis, which leads to periodic flavor oscillations among propagating neutrinos. The oscillation length is given by

$$\begin{aligned} \lambda_V &= \frac{4\pi E}{\delta m_{jk}^2} \\ &= 0.036 \left( \frac{E}{\text{GeV}} \right) \left( \frac{10^{-4} \text{ eV}^2}{\delta m_{jk}^2} \right) R_\odot, \end{aligned} \quad (6)$$

where  $\delta m_{jk}^2 \equiv m_j^2 - m_k^2$  denotes the neutrino mass-squared differences. As mentioned in Sec. I, the values of  $\delta m_{jk}^2$  inferred from solar and atmospheric neutrino-oscillation experiments are  $\delta m_{21}^2 \sim 10^{-4} \text{ eV}^2$  and  $\delta m_{32}^2 \sim 10^{-3} \text{ eV}^2$ , respectively. Thus, the vacuum oscillation lengths are well contained within the Sun for energies below 30 GeV.

The transformation between the mass basis and the flavor basis is described by the vacuum mixing matrix  $U_{\alpha j} = \langle j|\alpha\rangle = \langle \alpha|j\rangle^*$  with  $\alpha = e, \mu, \tau$  and  $j = 1, 2, 3$ . The conventional parametrization of the vacuum mixing

matrix invokes three angles and a phase [25]:

$$U = R_{23}(\theta_{23}) U_\delta^\dagger R_{13}(\theta_{13}) U_\delta R_{12}(\theta_{12}), \quad (7)$$

where  $R_{jk}(\theta_{jk})$  determines a rotation in the  $jk$  plane by an angle  $\theta_{jk}$ . The phase matrix

$$U_\delta = \begin{pmatrix} e^{i\delta/2} & 0 & 0 \\ 0 & 1 & 0 \\ 0 & 0 & e^{-i\delta/2} \end{pmatrix} \quad (8)$$

may be thought of as complexifying  $R_{13}(\theta_{13})$  to

$$\begin{aligned} R_{13}(\theta_{13}, \delta) &\equiv U_\delta^\dagger R_{13} U_\delta \\ &= \begin{pmatrix} \cos \theta_{13} & 0 & e^{-i\delta} \sin \theta_{13} \\ 0 & 1 & 0 \\ -e^{+i\delta} \sin \theta_{13} & 0 & \cos \theta_{13} \end{pmatrix}. \end{aligned} \quad (9)$$

We have omitted two additional Majorana phases, as they leave unaffected neutrino oscillations.

As mentioned before, the central values of the mixing angles inferred from oscillation experiments are quite consistent with the tribimaximal angles [20] given explicitly by  $\theta_{32} = 45^\circ$ ,  $\theta_{21} = 35.26\dots^\circ$ , and  $\theta_{13} = 0$ . The full tribimaximal mixing matrix is

$$U = \begin{pmatrix} \sqrt{\frac{2}{3}} & \sqrt{\frac{1}{3}} & 0 \\ -\sqrt{\frac{1}{6}} & \sqrt{\frac{1}{3}} & \sqrt{\frac{1}{2}} \\ -\sqrt{\frac{1}{6}} & \sqrt{\frac{1}{3}} & -\sqrt{\frac{1}{2}} \end{pmatrix}. \quad (10)$$

We remind the reader that rows are labeled from top to bottom by the flavor indices  $e$ ,  $\mu$ , and  $\tau$ , and columns are labeled left to right by mass-eigenstate indices 1, 2, and 3.

Due to decoherence of the propagating neutrino phases, we shall see that it is the classical probabilities  $|U_{\alpha j}|^2$ , obtained by squaring the mixing-matrix elements, that are of interest to us. We collect these squared elements into a matrix that we denote as  $\underline{U}$ . For tribimaximal mixing, its explicit form is

$$\underline{U} \equiv \frac{1}{6} \begin{pmatrix} 4 & 2 & 0 \\ 1 & 2 & 3 \\ 1 & 2 & 3 \end{pmatrix}. \quad (11)$$

One cannot avoid noticing the simplicity of the tribimaximal probabilities: the  $\nu_e$  contents of  $\nu_1$ ,  $\nu_2$ , and  $\nu_3$  are  $2/3$ ,  $1/3$ , and  $0$ , respectively, with the remaining probability being shared equally between  $\nu_\mu$  and  $\nu_\tau$ .

The  $3\text{-}\sigma$  experimental limits on the mixing-angle ranges are [26]

$$0.34 \leq \sin^2 \theta_{32} \leq 0.68, \quad (12)$$

$$0.24 \leq \sin^2 \theta_{21} \leq 0.41, \quad (13)$$

$$\sin^2 \theta_{13} \leq 0.044, \quad \text{or} \quad \theta_{13} \leq 12^\circ. \quad (14)$$

Notice that with  $\underline{U}_{e3} = \sin^2 \theta_{13}$ , the ‘‘zero’’ in  $\underline{U}$  may be as large as 4%. Later in this paper we will explore the sensitivity of our results to experimentally allowed variations in  $\theta_{13}$ .

Neglecting matter effects, the density matrix for neutrino production in the Sun is

$$\begin{aligned} \rho &= w_e |e\rangle\langle e| + w_\mu |\mu\rangle\langle \mu| + w_\tau |\tau\rangle\langle \tau| \\ &= \sum_\alpha w_\alpha U_{\alpha j}^* U_{\alpha k} |j\rangle\langle k|, \end{aligned} \quad (15)$$

where the weights  $w_\alpha$  are the relative flavor ratios at production normalized to obey  $w_e + w_\mu + w_\tau = 1$ . The density matrix for antineutrino production is given by the same formula when the  $w_\alpha$  are replaced with antineutrino production weights  $w_{\bar{\alpha}}$ . The first and second expressions in Eq. (15) present the production density matrix in the flavor and mass bases, respectively. The point of exhibiting  $\rho$  in the mass basis is twofold. First, this basis diagonalizes the free-neutrino Hamiltonian and is therefore appropriate for describing neutrino propagation to Earth. Second, it facilitates a discussion of decoherence, as is explained next.

As the neutrinos propagate from the Sun to the Earth, each off-diagonal operator  $|j\rangle\langle k|$  acquires a phase factor  $\exp(-i\phi_{kj})$  with large phase  $\phi_{kj} = L \delta m_{kj}^2 / 2E$ , where  $L$  is the distance from neutrino-production site to the detection site at Earth. The size of the Sun’s DM core and the detector’s size contribute a large  $\delta L$ , and energy resolution in the detector contributes a  $\delta E$  to the variance in the phase. For a statistical sample of events, these uncertainties randomize the phases, effectively equating the phase factor to its mean value  $\langle \exp(-i\phi_{kl}) \rangle = 0$ . Thus, off-diagonal elements of  $\rho$ , associated with the initial coherence of the neutrino wave function, may be dropped. The loss of phase information allows us to work with classical probabilities. We effectively obtain

$$\rho(\text{Earth}) = \sum_\alpha w_\alpha |U_{\alpha j}|^2 |j\rangle\langle j| \quad (16)$$

for the density matrix describing neutrinos arriving at Earth.

With the above result, the flavor probabilities at Earth are given by

$$P_{\nu_\alpha \rightarrow \nu_\beta} = \langle \beta | \rho(\text{Earth}) | \beta \rangle = \sum_{\alpha, j} w_\alpha |U_{\alpha j}|^2 |U_{\beta j}|^2. \quad (17)$$

In matrix form, this equation becomes

$$\begin{pmatrix} P_{\nu_\alpha \rightarrow \nu_e} \\ P_{\nu_\alpha \rightarrow \nu_\mu} \\ P_{\nu_\alpha \rightarrow \nu_\tau} \end{pmatrix} = \underline{U} \underline{U}^T \begin{pmatrix} w_e \\ w_\mu \\ w_\tau \end{pmatrix}. \quad (18)$$

Inputting the tribimaximal values leads to the explicit ‘‘flavor-propagation matrix’’

$$\underline{U} \underline{U}^T = \frac{1}{18} \begin{pmatrix} 10 & 4 & 4 \\ 4 & 7 & 7 \\ 4 & 7 & 7 \end{pmatrix}, \quad (19)$$

and to

$$\begin{aligned} P_{\nu_{\odot} \rightarrow \nu_e} &= \frac{1}{18} [10 w_e + 4(w_\mu + w_\tau)] \\ &= \frac{1}{9} (2 + 3 w_e), \end{aligned} \quad (20)$$

$$\begin{aligned} P_{\nu_{\odot} \rightarrow \nu_\mu} &= P_{\nu_{\odot} \rightarrow \nu_\tau} = \frac{1}{18} [4 w_e + 7(w_\mu + w_\tau)] \\ &= \frac{1}{18} (7 - 3 w_e). \end{aligned} \quad (21)$$

The equations for antineutrino flavor probabilities are obtained from these neutrino results via the replacement  $w_\alpha \rightarrow w_{\bar{\alpha}}$ .

In Eq. (21), the two probabilities  $P_{\nu_{\odot} \rightarrow \nu_\mu}$  and  $P_{\nu_{\odot} \rightarrow \nu_\tau}$  are equal. Also, in the first expressions on the right in Eqs. (20) and (21),  $w_\mu$  and  $w_\tau$  enter symmetrically. These results are manifestations of a  $\nu_\mu$ - $\nu_\tau$  interchange symmetry inherent in the tribimaximal mixing matrix. The  $\nu_\mu$ - $\nu_\tau$  interchange symmetry is exact for  $\theta_{23} = 45^\circ$  (maximal  $\nu_\mu$ - $\nu_\tau$  mixing) and  $\theta_{13} = 0$  [27]. The interchange symmetry holds in matter as well as in vacuum because the  $\nu_\mu$ - $\nu_\tau$  sector remains unaffected by the matter potential. More manifestations of the interchange symmetry will become evident in expressions and figures to be presented in subsequent sections. In the second expressions on the right in Eqs. (20) and (21),  $w_e + w_\mu + w_\tau = 1$  has been implemented. It is because of the  $\nu_\mu$ - $\nu_\tau$  interchange symmetry that the final result depends on the single weight  $w_e$ . This greatly reduces the latitude in characterizing the flavor distribution at the source.

For neutrinos with energies well below any matter resonances, the matter effects are negligible. These neutrinos therefore propagate as if in vacuum, and for tribimaximal mixing they produce flavor probabilities at Earth given by the formulas above. At higher energies, matter effects become substantial. One test for the efficacy of the solar matter potential on neutrino mixing would be to determine flavor probabilities with values *other* than those presented in Eqs. (20) and (21).

## B. Oscillations with matter: adiabatic approximation

In matter, the forward scattering amplitude of the neutrino leads to an effective potential [14]. The scattering amplitudes common to all neutrino flavors generate a common potential, which is unobservable in neutrino oscillations. However, there is a scattering amplitude unique to  $\nu_e$  and  $\bar{\nu}_e$  flavors. It is the  $W$ -exchange diagram for scattering on background electrons, with exchanges in the  $t$ -channel for  $\nu_e$  and in the  $s$ -channel for  $\bar{\nu}_e$ . Thus, there results an effective potential for the  $\nu_e$  and  $\bar{\nu}_e$  flavor states, given by  $V_e(r) = \sqrt{2} G_F n_e(r)$  for  $\nu_e$ , and  $-V_e$  for  $\bar{\nu}_e$ , where  $n_e$  is the electron number density. The effect of the matter contribution on neutrino flavor mixing

is best found by first transforming the vacuum Hamiltonian (5) to the flavor basis, labeled by  $\{|e\rangle, |\mu\rangle, |\tau\rangle\}$ , and then adding to this the flavor-diagonal effective potential. Then, the flavor-basis effective Hamiltonian in matter

$$H_F = U \frac{\text{diag}(-\delta m_{21}^2, 0, \delta m_{32}^2)}{2E} U^\dagger + V_e \text{diag}(1, 0, 0) \quad (22)$$

emerges. In Eq. (22), some contributions to  $H_F$  proportional to the identity have been omitted for convenience because they leave unchanged the flavor mixing, as explained earlier. For antineutrinos, the sign of matter-potential term is reversed and  $U$  is replaced by  $U^*$ .

The matrix that diagonalizes the flavor Hamiltonian in the matter background is called  $U_m$ :  $H_M = U_m^\dagger H_F U_m$ . Such a matrix is only fixed modulo the ordering and the phases of its column vectors. The phases are without physical significance because they can be absorbed into the definition of the states  $|j, r\rangle$  defined below. The ordering of the column vectors, on the other hand, determines the order of the eigenvalues along the diagonal of  $H_M$ . Our convention is this: the order of the column vectors in  $U_m$  is such that the diagonal entries of  $H_M$  exhibit the same ordering in magnitude as those of the matrix  $\hat{M} = \text{diag}(-\delta m_{21}^2, 0, \delta m_{32}^2)$  in Eq. (22). Note that this convention depends on the mass hierarchy, via the sign of  $\delta m_{32}^2$ . This convention is chosen such that  $U_m$  can smoothly approach the vacuum mixing matrix  $U$  in the limit of vanishing matter potential.

Given a position-dependent matter potential, the mixing matrix  $U_m(r)$  will also depend on position. For the matrix which diagonalizes  $H_F$  at the Sun's center, we reserve the notation  $U_m$  without argument  $r$ . In the solar core, the matter density plateaus, and the matter potential at the Sun's center is

$$V_e(0) = 70 \sqrt{2} G_F N_A \text{cm}^{-3} = 5.6 \times 10^{-12} \text{eV}. \quad (23)$$

Thus, neutrinos from the solar core with energy above  $\sim \delta m_{jk}^2/2V_e(0) \sim (\delta m_{jk}^2/10^{-5} \text{eV}^2) \text{MeV}$  will feel the effect of the Sun's matter potential. This class includes the  $E \gtrsim \text{GeV}$  neutrinos from WIMP annihilation.

With the mixing matrix in matter  $U_m(r)$  and the flavor eigenstates at hand, one can construct the ‘‘instantaneous’’ eigenstates of  $H_F$  via  $|j, r\rangle = U_m^\dagger(r)|\alpha\rangle$ . Although these states are strictly speaking not solutions to the equations of motion, they will turn out to be invaluable in what follows. For future reference, we further define the set of ‘‘matter states’’  $\{|1\rangle_m, |2\rangle_m, |3\rangle_m\}$  as the exact solution of the Schrödinger Equation with the Hamiltonian  $H_F$  given in Eq. (22). It is typically difficult to determine explicit expressions for these states. In this section, we simply note that equating  $|j\rangle_m$  to  $|j, r\rangle$  is known as the ‘‘adiabatic approximation.’’ We defer to Sec. II B 4 a more detailed discussion of this approximation. To summarize, the weak-interaction Hamiltonian is diagonal in the flavor basis  $|\alpha\rangle$ . On the other hand, the free-neutrino Hamiltonian in vacuum or matter is diagonal in the mass basis  $|j\rangle$  or the matter basis  $|j\rangle_m$ ,

respectively. An approximation for the matter states is given by the instantaneous eigenstates  $|j, r\rangle$ .

### 1. Diagonalization of $H_F$ for $\theta_{13} = 0$

The diagonalization of  $H_F$  is simplified by the observational input that  $\theta_{13}$  is small, so we can initially approximate it by zero. Then, the  $3 \times 3$  vacuum mixing matrix simplifies to  $U = R_{23}(\theta_{23}) R_{12}(\theta_{12})$ . This permits us to cast  $H_F$  into block-diagonal form via the transformation  $H'_F \equiv R_{23}^{-1}(\theta_{23}) H_F R_{23}(\theta_{23})$  because the rotation matrix  $R_{23}$  commutes with the matter-potential term in Eq. (22). The result is

$$H'_F = \begin{pmatrix} H_{2 \times 2} & 0 \\ 0 & \frac{\delta m_{32}^2}{2E} \end{pmatrix}, \quad (24)$$

with

$$H_{2 \times 2} = \begin{pmatrix} V_e(r) - \frac{\delta m_{21}^2}{2E} \cos^2 \theta_{12} & \frac{\delta m_{21}^2}{4E} \sin 2\theta_{12} \\ \frac{\delta m_{21}^2}{4E} \sin 2\theta_{12} & -\frac{\delta m_{21}^2}{2E} \sin^2 \theta_{12} \end{pmatrix} \quad (25)$$

determining the upper  $2 \times 2$  block. Note that the matter potential  $V_e(r)$  and off-diagonal elements are confined to  $H_{2 \times 2}$ . This means that the  $|3\rangle_m$  mass eigenstate in matter is unaffected by background electrons and decouples from the other two states. This allows a two-state treatment of the original three-flavor problem leading to some simplifications, which we discuss next.

Since the state  $|3\rangle_m$  is unaffected by the background matter, it is identical to the vacuum mass eigenstate  $|3\rangle = (R_{23}^{-1})_{3\alpha} |\nu_\alpha\rangle = \sin \theta_{23} |\mu\rangle + \cos \theta_{23} |\tau\rangle$ . The fact that  $|3\rangle_m = |3\rangle$  decouples from the other two states implies that the currently unknown neutrino mass hierarchy ( $m_3 > m_2 > m_1$  vs.  $m_2 > m_1 > m_3$ ) is unimportant in the present case characterized by  $\theta_{13} = 0$ .

Another simplification following from the three- to two-state reduction is the elimination of any possible CP-violation from the effective mixing matrix. This is evident in that the phase  $\delta$  does not enter into Eqs. (24) and (25). Still, the neutrino and antineutrino cases have to be treated separately, for their respective Hamiltonians differ in the sign of the matter-potential term.

A third simplifying feature arising from the reduction to two-state mixing is the straightforward recognition of a resonance condition. Mixing becomes resonant (maximal angle and degenerate eigenvalues) when the two diagonal elements of  $H_{2 \times 2}$  become equal, i.e., when

$$E_R(r) = \delta m_{21}^2 \cos 2\theta_{12} / 2 V_e(r). \quad (26)$$

The resonant energy at the Sun's center is therefore

$$E_R(0) = \cos 2\theta_{12} (\delta m_{21}^2 / 10^{-4} \text{eV}^2) 10 \text{ MeV}. \quad (27)$$

The tribimaximal value for  $\cos 2\theta_{12}$  is  $1/3$ . Equation (1) implies that outside the solar core the matter potential decreases, so that the resonance energy increases. Thus, only neutrinos with energies exceeding the solar-core value (27) can experience resonant conversion. The sign of  $\delta m_{21}^2$  is fixed as positive by solar data. It follows that for antineutrinos the right-hand side of Eq. (26) is negative, and there is no possibility of resonance conversion when  $\theta_{13} = 0$ .

The next step is to determine the eigenstates  $|1\rangle_m$  and  $|2\rangle_m$  of the effective  $2 \times 2$  Hamiltonian (25). Following the conventional analysis [29], we approximate these states by the instantaneous eigenvectors  $|1, r\rangle$  and  $|2, r\rangle$  that diagonalize  $H_{2 \times 2}$  at the point  $r$ . This adiabatic approximation is valid if the matter density changes slowly enough with distance. In this section, we assume adiabaticity holds. In the next section, we relax this assumption.

In the limit

$$E \gg \delta m^2 / 2 V_e(0), \quad (28)$$

the instantaneous eigenstate  $|1, 0\rangle$  at the Sun's core  $r \simeq 0$  is predominantly determined by the matter potential, leading to  $|1, 0\rangle \simeq |e\rangle$ . The majority of neutrinos from solar WIMP annihilation are expected to have energies  $E \gtrsim \mathcal{O}(\text{GeV})$ ; for these neutrinos,  $|1, 0\rangle \simeq |e\rangle$  is a good approximation [28]. Then the only mixing is due to  $\theta_{23}$  and we have  $U_m = R_{23}(\theta_{23})$  [28]. Thus, the remaining instantaneous mass state is given by  $|2, 0\rangle \simeq \cos \theta_{23} |\mu\rangle - \sin \theta_{23} |\tau\rangle$ .

As for the vacuum case in the previous subsection, we employ a density-matrix analysis to predict the flavor evolution. We again begin with the density matrix  $\rho(0)$  describing the mixed-flavor ensemble produced at the solar core. Our above considerations regarding the instantaneous mass states at the Sun's center yield [28]

$$\begin{aligned} \rho(0) &= w_e |e\rangle\langle e| + w_\mu |\mu\rangle\langle \mu| + w_\tau |\tau\rangle\langle \tau| \\ &= w_e |1, 0\rangle\langle 1, 0| + w_\mu \left( \frac{|3\rangle + |2, 0\rangle}{\sqrt{2}} \right) \left( \frac{\langle 3| + \langle 2, 0|}{\sqrt{2}} \right) \\ &\quad + w_\tau \left( \frac{|3\rangle - |2, 0\rangle}{\sqrt{2}} \right) \left( \frac{\langle 3| - \langle 2, 0|}{\sqrt{2}} \right). \end{aligned} \quad (29)$$

In the latter expression, the best-fit value of  $\theta_{23} \simeq 45^\circ$  has been implemented.

We continue by studying the propagation of the neutrinos from the Sun's core to its surface. Quantum interference effects can be safely neglected because the neutrinos quickly decohere after production: With the exception of possible resonance points  $r_{\text{res}}$  where the two eigenvalues of  $H_{2 \times 2}$  approach each other, the oscillation lengths  $\lambda$  are small compared to solar scales. For example, in the production region  $r \simeq 0$ , the set of approximate instantaneous eigenvalues of  $H'_F$  is  $\{-\delta m_{12}^2/2E, \delta m_{32}^2/2E, V_e(0)\}$ . The relative sizes of  $\delta m_{32}^2/2E$  and  $V_e(0)$  dominate, so that the oscillation scale is given by  $E/\delta m_{32}^2 \lesssim \mathcal{O}(100 \text{ km})$  for  $E > 1 \text{ GeV}$ ,

$\delta m_{32}^2 \approx 10^{-3} \text{eV}^2$ , and  $V_e^{-1}(0) \sim 40 \text{ km}$ . If the uncertainty in  $\delta L$  is comparable to these oscillation lengths, then the phase of the oscillation is randomized per neutrino and averaged out in the statistical sense. Such is the case here, since the size  $\sim 0.01 R_\odot \sqrt{100 \text{ GeV}/m_{\text{DM}}}$  of the WIMP annihilation region in the Sun's core [11] exceeds the oscillation scale of 100 km. Due to this decoherence, we can transform the density matrix  $\rho$  to the mass basis, and then disregard the off-diagonal pieces, as was done for the vacuum case. The result is three incoherent fluxes associated with the matter states  $|1, 0\rangle$ ,  $|2, 0\rangle$ , and  $|3\rangle$  emerging from the production region at the center of the Sun.

Neutrinos corresponding to  $|3\rangle$  will remain in this state because it is an exact eigenstate of the Hamiltonian unaffected by the solar electron density. However, the instantaneous eigenstates  $|1, r\rangle$  and  $|2, r\rangle$  change with respect to the flavor basis as  $r$  increases, and transitions between these states can occur. The adiabatic approximation neglects these transitions, so that a particle will remain in an instantaneous eigenstate. We note that the flavor-oscillation wavelengths for GeV neutrinos close to resonances in the Sun are long compared to the  $0.1 R_\odot$  scale length of the exponentially decreasing solar density, so that the adiabatic approximation breaks down in some circumstances. The adiabatic analysis presented here is nevertheless interesting, for it is instructive, simple, and applicable in certain energy ranges, as we shall see.

We are now in the position to establish the evolution of the density matrix. The discussion above shows that at sufficiently large neutrino energies the vacuum masses are negligible compared to the effective mass of the state  $|1, 0\rangle$ . However, outside the Sun, where  $V_e(r > R_\odot) = 0$ , the mass hierarchy is reversed: the instantaneous states are just the vacuum mass states  $|1, r > R_\odot\rangle = |1\rangle$  and  $|2, r > R_\odot\rangle = |2\rangle$  characterized by  $m_1 < m_2$ . Since the usual quantum-mechanical level repulsion prohibits level crossing, the states in the adiabatic approximation evolve as follows: as the neutrino travels to the solar surface, we have  $|1, 0\rangle \rightarrow |2\rangle$  and  $|2, 0\rangle \rightarrow |1\rangle$  up to phases [28]. As a result, we obtain the density matrix

$$\rho(r > R_\odot) = w_e |2\rangle\langle 2| + \frac{1}{2} (w_\mu + w_\tau) (|3\rangle\langle 3| + |1\rangle\langle 1|) \quad (30)$$

for neutrinos emerging from the Sun. Upon exiting the Sun, the  $|j\rangle$  states become exact eigenvectors of the neutrino Hamiltonian, so that transitions between these states cease to occur. Outside the Sun in empty space, the density matrix therefore remains effectively unchanged obeying  $\rho(\text{Earth}) = \rho(r > R_\odot)$ .

This result can be employed to determine the relative flavor fluxes measured in Earth-based experiments. The probability of detecting the neutrino flavor  $\beta \in \{e, \mu, \tau\}$  by such experiments is

$$\begin{aligned} P_{\nu_\odot \rightarrow \nu_\beta} &= \langle \beta | \rho(\text{Earth}) | \beta \rangle \\ &= w_e |U_{\beta 2}|^2 + \frac{1}{2} (w_\mu + w_\tau) (1 - |U_{\beta 2}|^2). \end{aligned} \quad (31)$$

In the final step, we have used  $\sum_{j=1}^3 |U_{\beta j}|^2 = 1$ , which arises from the unitarity of  $U$ . The  $\nu_\mu$ - $\nu_\tau$  interchange symmetry is evident again. The relation  $w_e + w_\mu + w_\tau = 1$  allows us to cast the expression in terms of  $w_e$  only. We remind the reader that although this result incorporates solar matter effects, the  $|U_{\beta j}|^2$  in the final expression are elements of the *vacuum* matrix  $\underline{U}$ .

Note that an amusing result emerges if  $|U_{e2}|^2 = |U_{\mu 2}|^2 = |U_{\tau 2}|^2$ , namely, that all three flavors arrive at Earth with equal probability  $1/3$ , *independent of the flavor ratios at production*. While  $|U_{e2}|^2 = |U_{\mu 2}|^2 = |U_{\tau 2}|^2$  may seem contrived, in fact it is the cornerstone of the tribimaximal mixing matrix. We discuss this next.

## 2. Neutrino flavor evolution

To obtain the expected neutrino flavor probabilities at Earth, we insert the tribimaximal mixing values for  $\underline{U}$  given in Eq. (11), into Eq. (31). Doing so, and using the normalization relation  $\sum_\alpha w_\alpha = 1$ , we arrive at

$$P_{\nu_\odot \rightarrow \nu_e} = P_{\nu_\odot \rightarrow \nu_\mu} = P_{\nu_\odot \rightarrow \nu_\tau} = \frac{1}{3}. \quad (32)$$

As advertised above, this result for neutrinos is independent of the  $w_\alpha$  which characterize the flavor distribution at the Sun's center. Such a result could hardly be simpler (or more democratic). It is easily understood as well: With the assumption that  $\theta_{13} = 0$ , the state  $|3\rangle$  is completely decoupled, and so the higher-energy resonance is absent. Thus, a  $\nu_e$  produced with energy above the lower-energy resonance emerges from the Sun as pure  $|\nu_2\rangle$  in the assumed adiabatic limit. With tribimaximal mixing, the decomposition of  $|\nu_2\rangle$  into flavors gives the observed ratios  $|U_{e2}|^2 : |U_{\mu 2}|^2 : |U_{\tau 2}|^2 = 1 : 1 : 1$ . On the other hand,  $\nu_\mu$ 's and  $\nu_\tau$ 's produced in the Sun's center equilibrate with each other, a consequence of the  $\nu_\mu$ - $\nu_\tau$  interchange symmetry. They then emerge from the Sun with equal parts of the two states orthogonal to  $\nu_2$ , i.e., with equal parts of  $\nu_1$  and  $\nu_3$ . The flavor decomposition of these states is  $|U_{\beta 1}|^2 + |U_{\beta 3}|^2 = 1 - |U_{\beta 2}|^2$ , which is again  $1 : 1 : 1$  for the tribimaximal mixing matrix. Thus,  $\nu_e$  and independently  $\nu_\mu$  and  $\nu_\tau$  generate a  $1 : 1 : 1$  flavor ratio at Earth. As a consequence, the  $1 : 1 : 1$  prediction is independent of the initial  $w_\alpha$ . The essence of this argument is visible in Eqs. (30) and (31).

Of course, the state evolution is not perfectly adiabatic, and  $\theta_{13}$  is probably not exactly zero. With either alteration, one expects deviation from the  $1 : 1 : 1$  flavor ratios. We address these issues in Sec. IIC. Figure 2 shows a comparison of our simplified approach described here with the full non-adiabatic result obtained in Sec. IIC.

We remark that the democracy derived above for the arriving neutrino flavors is a nontrivial prediction. First of all, it depends on the approximate validity of the tribimaximal mixing matrix. Second, it depends on the solar

matter, as outlined above. Reference to the vacuum predictions given in Eqs. (20) and (21) shows that without the solar-matter effect, flavor democracy results only for the single value  $\omega_e = 1/3$ . Third, even with tribimaximal mixing and the solar-matter effect, democracy is not a prediction for the arriving antineutrino flavors, as we show next.

### 3. Antineutrino flavor evolution

Antineutrinos from the Sun yield more interesting flavor probabilities. The construction of these flavor probabilities follows the same logic as those for neutrinos. However, there is one major difference: the hierarchy of the effective mass in the solar core and the vacuum mass hierarchy are identical, so that no mass-label permutation is necessary. To obtain the antineutrino analogue of Eq. (30), we must therefore take  $|1, 0\rangle \rightarrow |1\rangle$  and  $|2, 0\rangle \rightarrow |2\rangle$  in Eq. (29). This gives

$$P_{\bar{\nu}_\circ \rightarrow \bar{\nu}_\beta} = w_{\bar{e}} |U_{\beta 1}|^2 + \frac{1}{2} (w_{\bar{\mu}} + w_{\bar{\tau}}) (1 - |U_{\beta 1}|^2). \quad (33)$$

The tribimaximal mixing probabilities are  $|U_{e1}|^2 = \frac{2}{3}$  and  $|U_{\mu 1}|^2 = |U_{\tau 1}|^2 = \frac{1}{6}$ . It follows that

$$\begin{aligned} P_{\bar{\nu}_\circ \rightarrow \bar{\nu}_e} &= \frac{1}{6} (1 + 3w_{\bar{e}}), \\ P_{\bar{\nu}_\circ \rightarrow \bar{\nu}_\mu} &= P_{\bar{\nu}_\circ \rightarrow \bar{\nu}_\tau} = \frac{1}{12} (5 - 3w_{\bar{e}}). \end{aligned} \quad (34)$$

Here, the answer does depend on the flavor ratios  $w_{\bar{\alpha}}$  at production in the Sun's center. For example, an injection flux of purely  $\bar{\nu}_e$  leads to  $P_{\bar{\nu}_\circ \rightarrow \bar{\nu}_e} = \frac{2}{3}$  and  $P_{\bar{\nu}_\circ \rightarrow \bar{\nu}_\mu} = P_{\bar{\nu}_\circ \rightarrow \bar{\nu}_\tau} = \frac{1}{6}$ , whereas an injection flux with no  $\bar{\nu}_e$  leads to  $P_{\bar{\nu}_\circ \rightarrow \bar{\nu}_e} = \frac{1}{6}$  and  $P_{\bar{\nu}_\circ \rightarrow \bar{\nu}_\mu} = P_{\bar{\nu}_\circ \rightarrow \bar{\nu}_\tau} = \frac{5}{12}$ . Thus, in principle the  $w_{\bar{\alpha}}$  are measurable. Their determination would help unravel the nature of the DM source.

Why are the antineutrino flavor ratios not democratic, as were the neutrino ratios? The answer lies in the fact that  $\bar{\nu}_e$  emerges as pure  $\bar{\nu}_1$ , which is distributed in flavor as 4 : 1 : 1, and the  $\bar{\nu}_\mu$  and  $\bar{\nu}_\tau$  emerge as equal parts  $\bar{\nu}_2$  and  $\bar{\nu}_3$ , which are collectively distributed as 2 : 5 : 5. Thus, the resulting flavor ratios depend on the initial ratios  $w_{\bar{\alpha}}$ .

Since resonances in the antineutrino sector are absent within the normal hierarchy, another question arises. Why do the antineutrino results here differ from the vacuum results of Section II A? The difference is due to the mixing effect at the antineutrino production site. The large matter potential causes  $|e\rangle$  to be almost purely  $|1\rangle_m$ , whereas in vacuum  $|e\rangle$  would be distributed among the mass states  $|j\rangle$  as  $|U_{ej}|^2$ .

In Fig. 2, the approximate antineutrino probabilities derived here for adiabatic evolution and  $\theta_{13} = 0$  can be compared to the full analysis performed in the next section. It is seen in Fig. 2 that the simple approximation characterized by constant (i.e., energy-independent)

probabilities, is good over a relevant range of several decades in energy for the antineutrino.

We end this section with the remark that in both the neutrino and the antineutrino cases, all flavor probabilities converge to 1/3 (democratic 1 : 1 : 1) for  $w_e$  and  $w_{\bar{e}} = 1/3$ . This is because for these latter values all mass eigenstates are equally represented at production, and subsequent level repulsion simply permutes the labels of these mass states. This result holds for any values of the mixing matrix, and it also applies in the presence of matter effects, as we prove in Sec. II C 2.

### 4. Validity range of the above simplified results

As is evident in Fig. 2, for the normal mass hierarchy, the adiabatic approximation is good for neutrinos with energies between  $\sim 10$  MeV and  $\sim 10$  GeV, and for antineutrinos with energies above  $\sim 10$  MeV. What physics sets these limits of validity?

The low-energy limit of validity  $E_{\text{low}}$  is determined by the requirement that at production, the matter state  $|e\rangle$  be well separated from the other states; in turn, this requires that the matter-potential term dominates the vacuum mass term in the effective Hamiltonian (22) at production. A sufficient condition for this stipulation is given by Eq. (28), which yields  $E_{\text{low}} \simeq 70$  MeV when the value of  $\delta m_{32}^2$  is taken. In fact, the limit  $E_{\text{low}}$  can even be lower due to the particular form of the mixing matrices in the Hamiltonian (22).

At energies well below the lowest resonance, the matter term in the Hamiltonian becomes negligible and vacuum results are approached. As can be seen in Fig. 2, the low-energy asymptotes for all neutrino and antineutrino curves have the vacuum values given in Eqs. (20) and (21).

The high-energy limit of validity  $E_{\text{high}}$  is determined by the onset of non-adiabaticity, i.e., when appreciable transitions between the instantaneous eigenstates begin to occur. The non-adiabaticity scale  $\tilde{E}_{NA}$  is established in the next section. Borrowing results from the next section, we can conclude the following:  $\tilde{E}_{NA} \rightarrow \infty$  for the nonresonant  $\bar{\nu}$  case, and from Eq. (51),  $\tilde{E}_{NA} \sim 100$  GeV for the resonant  $\nu$  case with the parameters listed in Fig. 2.

Neutrino absorption in the Sun is significant at energies above  $\sim 100$  GeV, thus providing another limit on the validity of our analysis. If the absorption is universal across the flavors, then one might expect a reduction in flux and a change in spectrum, but little or no alteration of the flavor results we derive in this paper.

### 5. Neutrinos and antineutrinos together

An unmagnetized detector is ill-suited to resolve  $\nu$  events from  $\bar{\nu}$  events. For such a detector it is more



appropriate to consider the weighted average

$$\langle P_{\nu_{\odot} \rightarrow \nu_{\beta} \text{ or } \bar{\nu}_{\beta}} \rangle = \frac{\sigma_{\nu} F_{\nu_{\odot}} P_{\nu_{\odot} \rightarrow \nu_{\beta}} + \sigma_{\bar{\nu}} F_{\bar{\nu}_{\odot}} P_{\bar{\nu}_{\odot} \rightarrow \bar{\nu}_{\beta}}}{\sigma_{\nu} F_{\nu_{\odot}} + \sigma_{\bar{\nu}} F_{\bar{\nu}_{\odot}}} \quad (35)$$

as an observable. Here,  $F_{\nu_{\odot}}$  and  $F_{\bar{\nu}_{\odot}}$  are the neutrino and antineutrino fluxes produced by WIMP annihilation in the Sun, and  $\sigma_{\nu}$  and  $\sigma_{\bar{\nu}}$  are the neutrino and antineu-

trino cross sections in the detector. We define the neutrino to antineutrino cross-section ratio as  $r_{\sigma} \equiv \sigma_{\bar{\nu}}/\sigma_{\nu}$ . Experimentally,  $r_{\sigma} \sim 1/2$  in the energy range of interest. In situations in which neutrino production is charge symmetric, the initial  $\nu_{\alpha}$  and  $\bar{\nu}_{\alpha}$  fluxes are equal, as are  $w_{\alpha}$  and  $w_{\bar{\alpha}}$ . The weighted average of Eqs. (31) and (33) is then simply given by

$$\langle P_{\nu_{\odot} \rightarrow \nu_{\beta} \text{ or } \bar{\nu}_{\beta}} \rangle = \frac{[w_e (3 |U_{\beta 2}|^2 - 1) + 1 - |U_{\beta 2}|^2] + r_{\sigma} [w_e (3 |U_{\beta 1}|^2 - 1) + 1 - |U_{\beta 1}|^2]}{2(1 + r_{\sigma})} \quad (36)$$

Assuming the tribimaximal mixing angles, one obtains

$$\begin{aligned} \langle P_{\nu_{\odot} \rightarrow \nu_{\mu} \text{ or } \bar{\nu}_{\mu}} \rangle &= \langle P_{\nu_{\odot} \rightarrow \nu_{\tau} \text{ or } \bar{\nu}_{\tau}} \rangle = \frac{4 + r_{\sigma}(5 - 3w_e)}{12(1 + r_{\sigma})}, \\ \langle P_{\nu_{\odot} \rightarrow \nu_e \text{ or } \bar{\nu}_e} \rangle &= \frac{2 + r_{\sigma}(3w_e + 1)}{6(1 + r_{\sigma})}. \end{aligned} \quad (37)$$

The  $w_e$  dependence of these results, although weakened compared to the pure  $\bar{\nu}$  sample given in Eq. (34), implies that detectors that sum  $\nu$  and  $\bar{\nu}$  events still have some discriminatory power to resolve different source models. In Sec. III we discuss this possibility.

### 6. Summary of adiabatic evolution in matter

In our description of adiabatic evolution in matter, we adopted three simplifying assumptions governing neutrino (and antineutrino) production by solar WIMP annihilation, and subsequent propagation out of the Sun to Earth. These assumptions are that all neutrino energies exceed the resonant energy at the Sun's center ( $E_R(0) \sim 10$  MeV), that the neutrinos evolve adiabatically through the Sun, and that neutrino mixing angles are given by the tribimaximal values, including  $\theta_{13} = 0$ . As a consequence, we obtained energy-independent flavor probabilities for the neutrinos arriving at Earth. We learned that solar matter plays a significant role in determining the expected flavor ratios at Earth. However, the higher-energy resonant value  $E_R^h$  has yet to play a role, since  $\theta_{13} = 0$  decouples the  $|3\rangle$  state from the  $|1\rangle$  and  $|2\rangle$  states. In the next subsection, we relax the various assumptions.

### C. Non-adiabatic oscillations and nonzero $\theta_{13}$

The physics becomes more complicated when simplifying assumptions are abandoned. For example, if  $\theta_{13}$  is no longer assumed to be zero, then the state  $|3\rangle$  no longer decouples and a full three-flavor analysis with two resonant energies is typically required.

#### 1. Nonzero $\theta_{13}$ and three-flavor mixing

We begin again with the density matrix  $\rho_{\nu}(0)$  at production, expressed in flavor space:

$$\rho_{\nu}(0) = \sum_{\alpha} w_{\alpha} |\alpha\rangle\langle\alpha|, \quad (38)$$

where  $\alpha \in \{e, \mu, \tau\}$  runs over the three flavors, and the  $w_{\alpha}$  are the relative flavor fluxes at production, as before. Paralleling our previous simplified analysis, we expand the flavor eigenstates  $|\alpha\rangle$  in the basis of instantaneous eigenstates  $|j, r\rangle$  at  $r = 0$ , where  $j \in \{1, 2, 3\}$  labels again the effective-mass eigenvalue:  $|\alpha\rangle = \sum_j \langle j, 0 | \alpha \rangle |j, 0\rangle$ . We obtain

$$\rho_{\nu}(0) = \sum_{\alpha, j, k} w_{\alpha} (U_m)_{\alpha j} (U_m)_{\alpha k}^* |j, 0\rangle\langle k, 0|. \quad (39)$$

Recall the earlier definition of  $U_m$  as the solar-core instantaneous mixing matrix in matter, i.e.,  $(U_m)_{\alpha k} \equiv \langle \alpha | k, 0 \rangle$ . The matter at the Sun's center characterizes the core environment where the neutrinos are produced. Again, as so defined,  $U_m$  diagonalizes  $H_F$  only at the center of the Sun.

The same decoherence arguments presented in the previous section allow us again to neglect the off-diagonal density-matrix elements in Eq. (39). Therefore, in what follows we will take

$$\rho_{\nu}(0) = \sum_{\alpha, j} w_{\alpha} |(U_m)_{\alpha j}|^2 |j, 0\rangle\langle j, 0| \quad (40)$$

as the neutrino-production density-matrix. As a check, we note that with a large matter potential isolating the  $|\nu_e\rangle$  state and maximal  $\theta_{32} = 45^\circ$ , Eq. (40) becomes identical to our earlier Eq. (29).

#### 2. Non-adiabatic evolution

Next, we re-examine the evolution of this system during propagation to the solar surface, but this time without the adiabatic assumption of the previous section.

That is, we now allow for transitions between the instantaneous eigenstates  $|j, r\rangle$ .

Once the neutrinos reach the vacuum at the Sun's surface, transitions between the eigenstates  $|j, r > R_\odot\rangle = |j\rangle$  no longer occur because in free space the  $|j\rangle$  are exact eigenstates of the Hamiltonian. For our analysis, we are therefore interested in the solar-propagation amplitudes  $A_{kj} \equiv \langle k|j, 0\rangle$ . Embedded in these amplitudes are the important non-adiabatic transitions between instantaneous eigenstates, most likely to occur near resonance.

In terms of the amplitudes  $A_{kj}$ , the density matrix given in Eq. (40) evolves to become, beyond the Sun's surface,

$$\rho_\nu(r > R_\odot) = \sum_{\alpha, j, k, l} w_\alpha |(U_m)_{\alpha j}|^2 A_{lj}^* A_{kj} |k\rangle\langle l|. \quad (41)$$

It is seen here that non-adiabatic transitions replenish the off-diagonal elements of  $\rho$ . However, the  $A_{kj}$  in general contain position-dependent phases, which must be averaged over the production region. Furthermore, additional loss of phase information occurs as the neutrinos continue en route to Earth, as discussed in Sec. II A. So again the off-diagonal terms average to zero. Consequently, Eq. (41) is reduced to the more manageable expression

$$\rho_\nu(\text{Earth}) = \sum_{\alpha, j, k} w_\alpha |(U_m)_{\alpha j}|^2 |A_{kj}|^2 |k\rangle\langle k|. \quad (42)$$

The amplitude  $A_{jk}$  is seen to enter the final formula only via the jump probability  $P_{kj} \equiv |A_{kj}|^2$ , as expected in the absence of coherence.

Equation (42) can now be employed to determine the probability of detecting a neutrino of flavor  $\beta$  at Earth. We obtain

$$\begin{aligned} P_{\nu_\odot \rightarrow \nu_\beta} &= \langle \beta | \rho(\text{Earth}) | \beta \rangle \\ &= \sum_{\alpha, j, k} w_\alpha |(U_m)_{\alpha j}|^2 P_{kj} |U_{\beta k}|^2. \end{aligned} \quad (43)$$

In matrix form, this equation is given by

$$\begin{pmatrix} P_{\nu_\odot \rightarrow \nu_e} \\ P_{\nu_\odot \rightarrow \nu_\mu} \\ P_{\nu_\odot \rightarrow \nu_\tau} \end{pmatrix} = \underline{U} P \underline{U}_m^T \begin{pmatrix} w_e \\ w_\mu \\ w_\tau \end{pmatrix}. \quad (44)$$

Here, we have defined the matter matrix  $(\underline{U}_m)_{\alpha j} \equiv |(U_m)_{\alpha j}|^2$ , in analogy to our earlier vacuum definition Equations (43) and (44) generalize Eqs. (31) and (18) in the previous subsections. In the adiabatic ( $P_{kj} \rightarrow \delta_{kj}$ ) and matter-free ( $\underline{U}_m \rightarrow \underline{U}$ ) limits, these equations reduce to their analogues in the previous subsections.

With Eq. (43) at hand, we may establish rigorously an interesting feature of the flavor evolution: *If the flavors at production are democratically distributed ( $w_e = w_\mu = w_\tau = 1/3$ ), then the flavor probabilities observed at Earth will also be democratically distributed.* In other words, the particular ratio  $(\frac{1}{3}, \frac{1}{3}, \frac{1}{3})$  of flavors is left unchanged by the combination of all oscillation and matter

effects. This is expected in that off-diagonal density-matrix elements average to zero, so that the density-matrix evolves by changing bases, from flavor in matter to evolving mass in matter, to constant mass in vacuum, and finally to flavor at earth; but a density matrix proportional to the unit matrix initially, remains so throughout basis changes.

We verify this conclusion by setting  $w_\alpha = 1/3$  in Eq. (43), and rewriting the remaining terms slightly:

$$P_{\nu_\odot \rightarrow \nu_\beta} = \frac{1}{3} \sum_k |U_{\beta k}|^2 \sum_j P_{kj} \sum_\alpha |(U_m)_{\alpha j}|^2. \quad (45)$$

The unitarity of  $U_m$  implies that the sum over  $\alpha$  appearing on the far right-hand side of Eq. (45) equals unity. Similarly, the sum of elements in the row or column of  $P_{kj}$  must add up to 1 because of probability conservation. The remaining sum over  $k$  is also equal to 1 due to the unitarity of  $U$ . We are thus left with the claimed result that  $P_{\nu_\odot \rightarrow \nu_\beta} = \frac{1}{3}$  for all flavors  $\beta$ . Consequently, any experimentally inferred flavor ratios deviating from 1 : 1 : 1 exclude a democratic source.

Equation (43) allows predictions to be made for neutrino flavors at Earth, given an initial distribution of flavors in the solar core. It has been used extensively in the context of suppression of the expected solar  $\nu_e$  rate at Earth. For neutrinos from the solar fusion cycle, one has  $w_e = 1$ , with all other  $w_\alpha$  and  $w_{\bar{\alpha}}$  equal to zero. However, little study of Eq. (43) has been performed for an ensemble of solar flavors, as would arise from WIMP annihilation in the Sun. An early study of neutrino flavor physics arising from solar WIMP annihilation was performed in Ref. [15]. Much has been learned about the neutrino mixing matrix in the intervening fifteen years. We incorporate subsequent knowledge into our work here.

An approximation for  $\underline{U}_m$  is derived in Appendix A, so our remaining task is to present explicit expressions for the transition probabilities  $P_{kj} \equiv |A_{kj}|^2$ . In the adiabatic approximation of the previous section, these  $|A_{kj}|^2$  were just  $\delta_{kj}$ . However, the adiabatic approximation can break down in resonance regions, where the oscillation length increases by the factor  $1/\sin 2\theta$  in the two-state approximation. If the oscillation length becomes comparable to or larger than the scale length of the matter potential  $|d \ln V_e(r)/dr|^{-1}$ , the medium and therefore the matter-induced mixing angles are changing sufficiently fast, so that adiabaticity is violated [30]. When neutrino evolution is non-adiabatic,  $P_{kj}$  has a complicated structure and includes off-diagonal pieces. The nature of  $P_{kj}$  is discussed next.

For further progress, we employ another piece of experimental data:  $\delta m_{21}^2$  and  $\delta m_{32}^2$  differ by more than an order of magnitude, so that both resonances in our three-neutrino system can be treated separately and involve only two levels at a time [31]. For each of the two resonances, an improved Landau-Zener approximation

establishes a variant of the Parke formula [30]

$$P_c = \Theta(E - E_R(0)) \frac{\exp(-\Gamma \sin^2 \theta) - \exp(-\Gamma)}{1 - \exp(-\Gamma)} \quad (46)$$

as the generic leading-order form of the level-crossing probability [29]. Here,  $\theta$  is the effective two-level vacuum mixing angle,  $\Gamma$  is the ‘‘adiabaticity parameter’’, and  $E_R(0) \equiv E_R$  is the resonance energy at the solar core. These quantities depend upon the three-level vacuum neutrino parameters, the matter-density profile, and the resonance under consideration. Before applying Eq. (46) to each resonance in the present situation, we discuss some of its general features.

As discussed in Sec. II B 1, outside the Sun’s center the resonance energy increases  $E_R(r \neq 0) > E_R$ . It follows that only neutrinos produced with energies  $E > E_R$  can experience resonance conversion on their way to the Sun’s surface. Since a resonance is required for appreciable level-crossing probabilities, we need  $E > E_R$  in order for  $P_c \neq 0$ . This feature is ensured by the presence of the threshold function  $\Theta$  in Eq. (46). We also note that the crossing probability  $P_c$  goes smoothly to 100% as  $\theta$  approaches zero. This is expected and necessary; it reflects the fact that two states cannot repel each other when they are decoupled.

Explicit expressions for the adiabaticity parameter  $\Gamma$  show [29] that it depends on the neutrino energy as  $1/E$ . Thus, it is useful to define a ‘‘non-adiabatic energy’’  $\tilde{E}_{NA}$  via the simple equation

$$\Gamma \equiv \frac{\tilde{E}_{NA}}{E}; \quad (47)$$

$\tilde{E}_{NA}$  sets the energy scale for non-adiabatic effects. In the limit  $E \rightarrow 0$ ,  $\Gamma \rightarrow \infty$  and the crossing probability  $P_c$  goes to zero. This is the adiabatic limit. The onset of non-adiabaticity is found by expanding Eq. (46) under the condition  $E \ll \tilde{E}_{NA}$ . One has

$$P_c = \exp(-\Gamma \sin^2 \theta) - \exp(-\Gamma) + \dots \quad (48)$$

Taking  $P_c = e^{-3} \simeq 5\%$  as a characteristic value for the onset of non-adiabaticity, the leading term in Eq. (48) determines an onset energy  $E_{NA}$  for non-adiabatic effects:

$$E_{NA} = \frac{1}{3} \sin^2 \theta \tilde{E}_{NA}. \quad (49)$$

Thus we have an energy condition for nonadiabaticity:  $E > \max\{E_R, E_{NA}\}$ . Note, however, that for very large energy  $E \gg \tilde{E}_{NA}$ ,  $\Gamma$  goes to zero and  $P_c$  approaches  $\cos^2 \theta$ . This reflects the fact that at very high energies the oscillation wavelength exceeds the matter region, and so vacuum oscillations result.

For large  $\sin^2 \theta$ , the definition (49) may be inconsistent because the next-to-leading contribution in Eq. (48) can become sizable. However, we will see below that only the cases  $\theta = \theta_{12}, \theta_{13} < 45^\circ$  are of interest in the present context. The ratio of the second to first terms in the

expansion (48) evaluated at  $E_{NA}$  is  $\exp(-3 \cot^2 \theta)$ . Even for the ultra-conservative assumption  $\theta = 45^\circ$ , this ratio is less than 5%, so that Eq. (49) is more than sufficient for our purposes.

Although the generic crossing probability (46) provides the basis for the determination of  $P_{jk}$ , many details also depend on the number of resonances encountered (0, 1, or 2), the mass hierarchy, and on whether neutrinos or antineutrinos are considered. For example, with  $\theta_{13} = 0$  the state  $|3\rangle$  decouples as we have seen, and there is but a single resonance; it lies in the neutrino sector with either the normal or inverted mass hierarchies. With  $\theta_{13} \neq 0$ , there are two resonances; they both lie in the neutrino sector with the normal mass hierarchy, but lie one each in the neutrino and antineutrino sectors with the inverted mass hierarchy. The schematic Fig. 1 displays the possibilities. We use superscripts  $l$  and  $h$  on relevant variables to denote the lower- and higher-energy resonances, and  $+$  and  $-$  to denote the normal and inverted hierarchies, respectively. Some obvious energy regions where evolution is purely adiabatic are (i)  $E_\nu \lesssim E_{NA}^l$ , (ii) all  $E_{\bar{\nu}}$  with the normal hierarchy, (iii) all  $E_{\bar{\nu}}$  with the inverted hierarchy when  $\theta_{13} = 0$ , and (iv)  $E_{\bar{\nu}} \lesssim E_{NA}^h$  with the inverted hierarchy when  $\theta_{13} \neq 0$ . We will consider below the various cases, normal vs. inverted hierarchy, and  $\theta_{13}$  zero vs. nonzero.

In principle, a neutrino produced on the back side of the Sun but traveling toward us may encounter two resonances before leaving the production region. There is a standard formalism available to describe this physics [29]. However, we may ignore this ‘‘res-in-res-out’’ possibility for two reasons. The first is that the region of DM annihilation is expected to be so small ( $\lesssim 0.01 R_\odot$ ) that only neutrinos within a particular narrow energy band could encounter the resonances. The second reason is that the matter density within  $0.1 R_\odot$  of the solar core deviates from the exponential behavior in Eq. (1): it becomes nearly constant [23]. This near-constancy of the density profile holds even better within  $\lambda_{DM} \sim 0.01 R_\odot$ .

### 3. (Anti)Neutrino flavors – normal hierarchy

For the normal hierarchy  $\delta m_{32}^2 > 0$ , there are two resonances for neutrinos and none for antineutrinos. The lower-energy neutrino resonance occurs between the two lightest states. For this situation, the characteristic quantities  $E_R$ ,  $\tilde{E}_{NA} = \Gamma E$ , and  $\theta$  in the crossing-probability formula (46) are given by [29, 32]

$$\begin{aligned} E_R^{l+} &= \frac{\delta m_{21}^2 \cos 2\theta_{12}}{2V_e(0) \cos^2 \theta_{13}}, \\ \tilde{E}_{NA}^{l+} &= \Gamma E = \pi \left| \frac{V_e}{V'_e} \right|_{r_R} \delta m_{21}^2, \\ \theta^{l+} &= \theta_{12}. \end{aligned} \quad (50)$$

These expressions are valid at leading order. Appropriate to the case which we are discussing, the superscripts  $l$

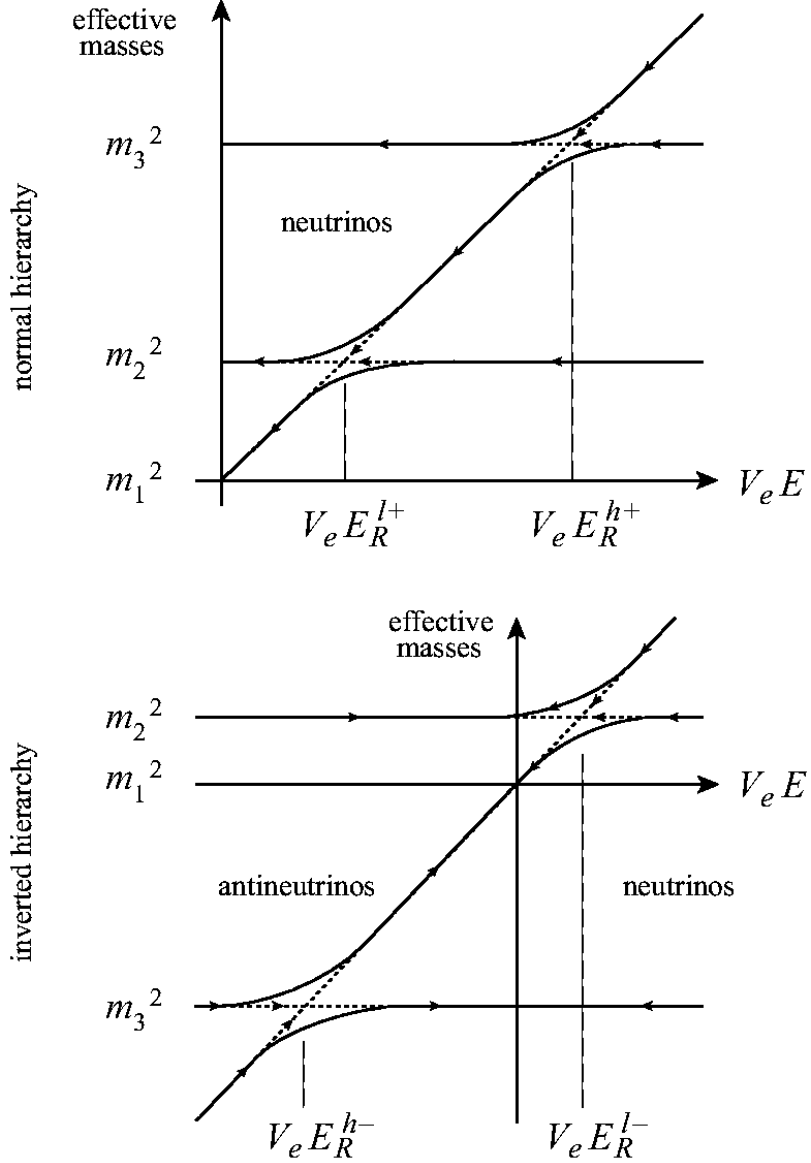


FIG. 1: Schematic illustration of the relative positions of the lower- and higher-energy resonances for the normal and inverted mass hierarchies. Neutrino (antineutrino) eigenvalues are on the right (left) of the vertical effective-mass axis. The dotted lines indicate non-adiabatic transitions.

and + label the lower-energy resonance and the normal hierarchy with  $\delta m_{32}^2 > 0$ ,

The logarithmic derivative inside the absolute-value sign is to be evaluated at the radial position  $r_R$  of the respective resonance. In the present case of an exponential density profile, this factor is equal to  $\lambda_\odot \sim 0.1 R_\odot$  and independent of  $r$ , which simplifies the analysis. In particular, we may set

$$\tilde{E}_{NA}^{l+} = \pi \lambda_\odot \delta m_{21}^2 \simeq 110 \text{ GeV} \frac{\delta m_{21}^2}{10^{-4} \text{ eV}^2}. \quad (51)$$

The corresponding expression for the onset of non-

adiabaticity (49) in the present case is

$$E_{NA}^{l+} = \frac{1}{3} \sin^2 \theta_{12} \tilde{E}_{NA}^{l+}. \quad (52)$$

For the higher-energy neutrino resonance occurring between the two heaviest states, the characteristic quantities  $E_R$ ,  $\tilde{E}_{NA}$ , and  $\theta$  are given at leading order by [29, 33]

$$\begin{aligned} E_R^{h+} &= \frac{\delta m_{32}^2 + \delta m_{21}^2 \cos^2 \theta_{12}}{2V_e(0)} \cos 2\theta_{13}, \\ \tilde{E}_{NA}^{h+} &= \pi \left| \frac{V_e}{V_e'} \right|_{r_R} (\delta m_{32}^2 + \delta m_{21}^2 \cos^2 \theta_{12}), \\ \theta^{h+} &= \theta_{13}, \end{aligned} \quad (53)$$

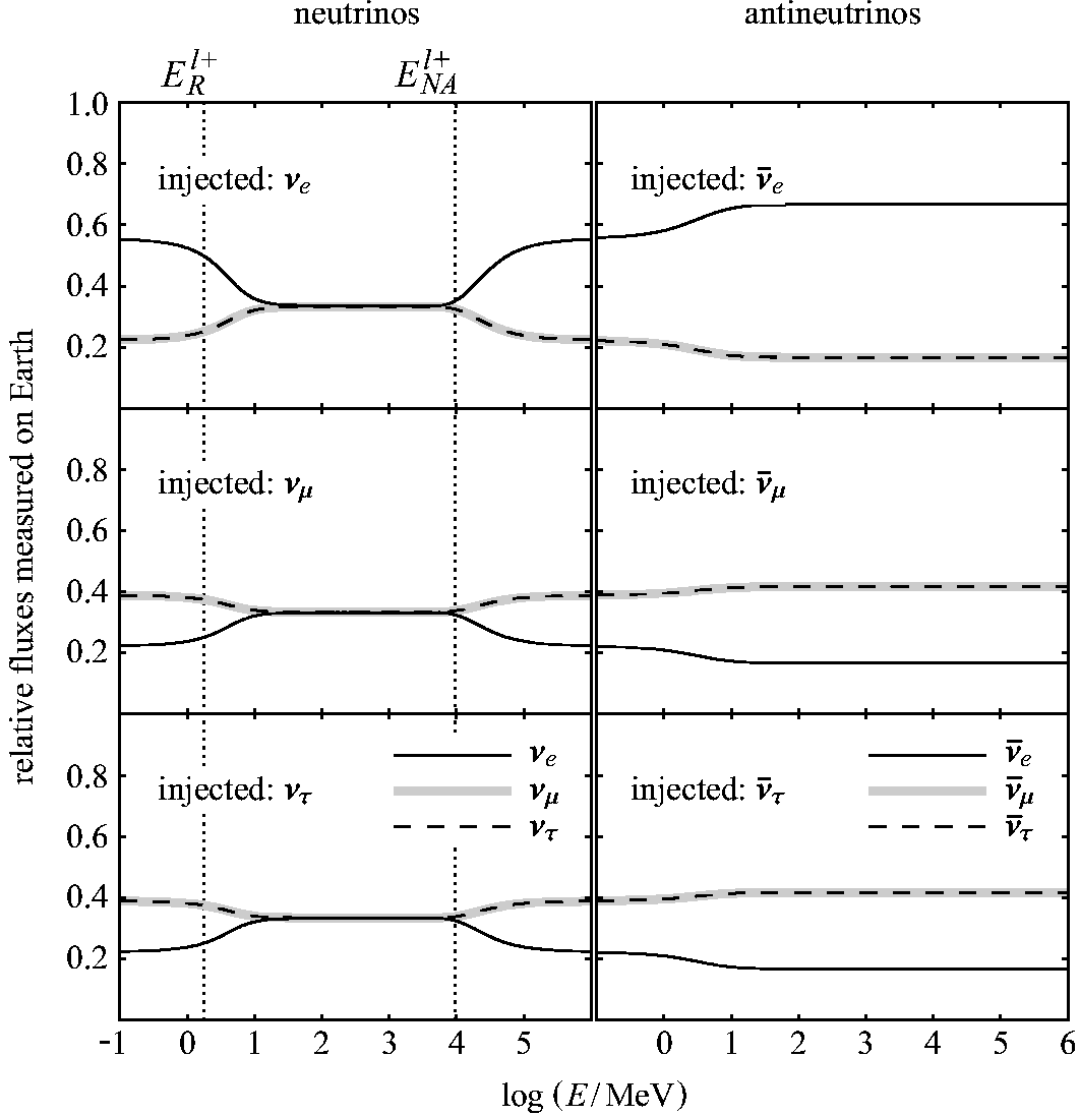


FIG. 2: Solar neutrino and antineutrino flavor probabilities at Earth versus energy, for a single injection flavor and for the normal mass hierarchy. The  $\nu_e$ ,  $\nu_\mu$ , and  $\nu_\tau$  spectra at Earth are shown as solid, gray, and dashed lines. The neutrino mass-squared differences are  $\delta m_{21}^2 = 8.0 \times 10^{-5} \text{ eV}^2$  and  $\delta m_{32}^2 = 3.0 \times 10^{-3} \text{ eV}^2$ , and the mixing angles are  $\theta_{12} = 35^\circ$ ,  $\theta_{13} = 0^\circ$ , and  $\theta_{23} = 45^\circ$ . The CP-violating phase  $\delta$  is set to zero. The vertical dotted lines mark the characteristic scales for the lower-energy resonance given in Eqs. (50) and (52). There is no higher-energy resonance when  $\theta_{13} = 0$ . Note the  $\nu_\mu$ - $\nu_\tau$  and  $\bar{\nu}_\mu$ - $\bar{\nu}_\tau$  interchange symmetries discussed in the text. Because  $\theta_{13}$  is set to zero here, these results remain valid also for the inverted-hierarchy case. Note that the high-energy neutrino fluxes are identical to the low-energy antineutrino fluxes. This accidental feature is attributable to tribimaximal mixing, as explained in Appendix B.

where the superscript  $h+$  labels the present higher-energy resonance, normal-hierarchy situation. From Eq. (49), we obtain here

$$E_{NA}^{h+} = \frac{1}{3} \sin^2 \theta_{13} \tilde{E}_{NA}^{h+} \quad (54)$$

for the onset of non-adiabaticity.

We now assemble all the pieces necessary for including non-adiabatic matter effects into our analysis for the normal-hierarchy case. The neutrino level-crossing prob-

abilities are determined by

$$P_{kj} = \begin{pmatrix} 1-P_c^l & P_c^l & 0 \\ P_c^l & 1-P_c^l & 0 \\ 0 & 0 & 1 \end{pmatrix} \begin{pmatrix} 1 & 0 & 0 \\ 0 & 1-P_c^h & P_c^h \\ 0 & P_c^h & 1-P_c^h \end{pmatrix}, \quad (55)$$

where the superscripts  $l$  and  $h$  imply evaluation of the crossing probability (46) at the lower resonance with Eqs. (50) and at the higher resonance with Eqs. (53), respectively. We remark that with two resonances at play,  $P_{jk} \neq P_{kj}$  in general, so that the ordering of the two non-commuting matrices on the right-hand side of Eq. (55) is

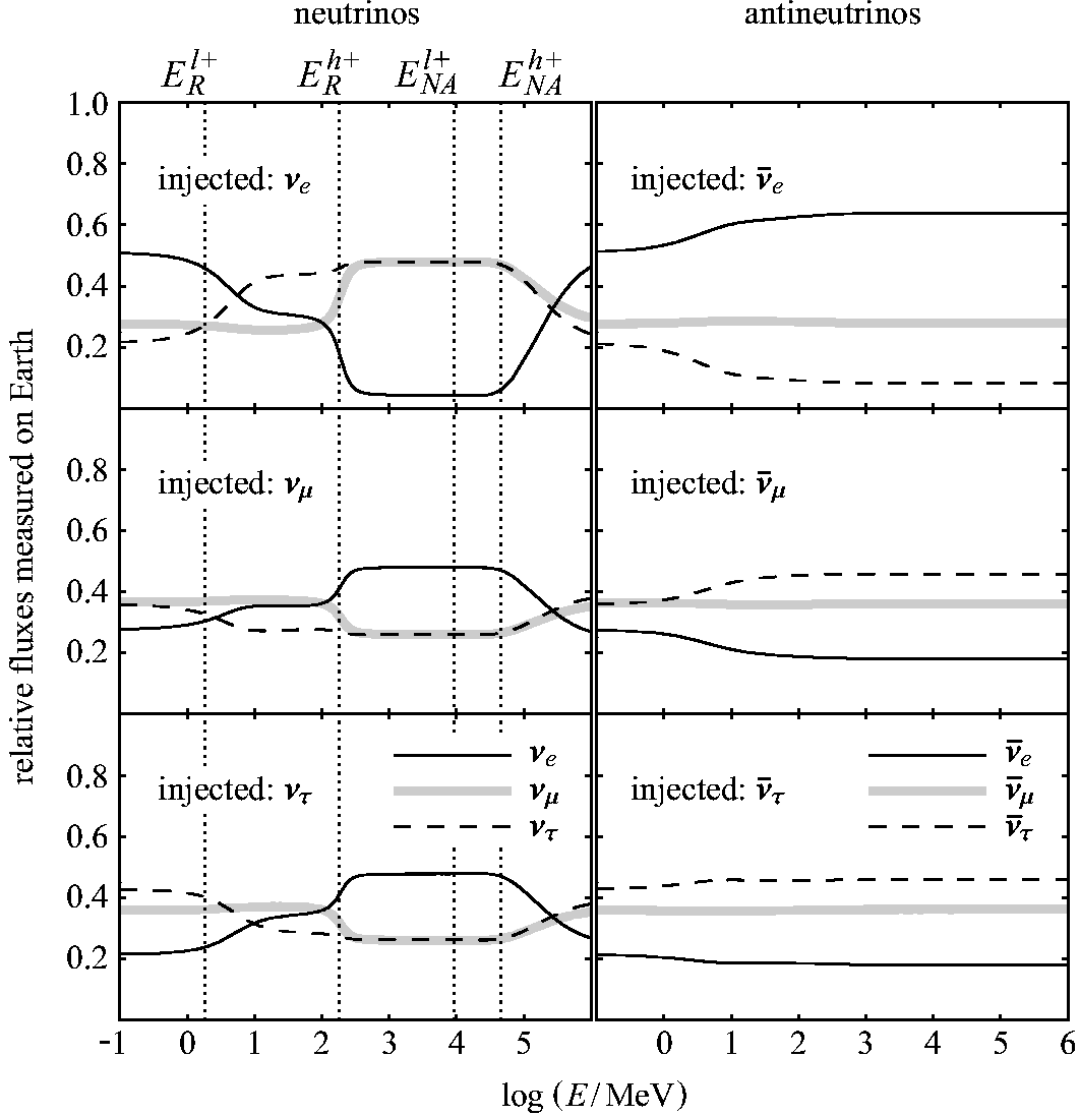


FIG. 3: Solar neutrino and antineutrino flavor probabilities at Earth versus energy, for a single injection flavor and for the normal mass hierarchy. Here, we have taken  $\theta_{13} = 12^\circ$ ,  $\delta = 0$ . All other neutrino parameters are as in Fig. 2. The  $\nu_\mu$  and  $\nu_\tau$  spectra and  $\bar{\nu}_\mu$  and  $\bar{\nu}_\tau$  spectra are interchanged if  $\delta = \pi$  is chosen. Vertical dotted lines mark the characteristic scales for the lower-energy resonance given by Eqs. (50) and (52) and the higher-energy resonance given by Eqs. (53) and (54).

essential.

On the other hand, for antineutrinos there are no resonances present in the normal-hierarchy case. The adiabatic relation  $P_{kj} = \delta_{kj}$  is exact.

The terrestrial flavor fluxes resulting from pure flavor injection in the Sun's center are plotted in Figs. 2 and 3 for representative sets of neutrino parameters. One sees that the processed flavors arriving at Earth are far from pure. The neutrino spectra in Fig. 2 illustrates the three energy regions that may result from the influence of a matter resonance. At  $E_\nu \gtrsim E_{NA}^{l+}$ , the flavor evolution is complicated by non-adiabaticity. In the region  $E_R^{l+} \lesssim E_\nu \lesssim E_{NA}^{l+}$ , the flavor ratios have the simple adiabatic values presented and discussed in Sec. II B 2. Below

$E_R^{l+}$ , the matter state  $|e\rangle$  is not well separated from the other states, and the description is again complicated. A simplifying feature for all energies is the  $\mu$ - $\tau$  degeneracy that necessarily results when  $\theta_{32} = 45^\circ$  and  $\theta_{13} = 0$ .

Figs. 2 and 3 differ in that the minimal  $\theta_{13} = 0$  is input into the first, and the 3- $\sigma$  maximal  $\theta_{13} = 12^\circ$  is input into the second. Several qualitative differences result when  $\theta_{13}$  is nonzero. The most noticeable is that with  $\theta_{13} \neq 0$ , the mixing between  $|3\rangle$  and an injected  $|e\rangle$  significantly suppresses the  $\nu_e$  flavor at Earth in the adiabatic high-energy region between  $E_R^{h+}$  and  $E_{NA}^{h+}$ . The next most noticeable change is the breaking of the  $\mu$ - $\tau$  degeneracy, for both neutrinos and antineutrinos. As explained in Sec. II C 6, the  $\nu_\mu$  and  $\nu_\tau$  spectra, and the  $\bar{\nu}_\mu$  and  $\bar{\nu}_\tau$

spectra, are interchanged if  $\delta = 0$  is replaced with  $\delta = \pi$ .

Although there are no antineutrino resonances with the normal hierarchy, there are nevertheless features in the antineutrino flavor spectrum at the resonant energies. These “kinematical reflections” are due to the following physics: As the energy passes from below to above the resonant value, the effective Hamiltonian (22) morphs from being vacuum dominated to being matter dominated. In turn, the mixing angle(s) associated with the resonance morph from their vacuum value(s) to their matter value(s). If the respective signs of the vacuum and matter parts of the Hamiltonian are opposite, as happens for neutrinos in the normal hierarchy, then the transition may be dramatic; at resonance the mixing angle passes through  $45^\circ$ . If instead, the signs of the two Hamiltonian pieces are the same, as with antineutrinos in the normal hierarchy, then the transition in mixing-angles is less dramatic, but possibly still significant. The transition of mixing angles through the lower resonant energy in the  $\bar{\nu}_e$  and  $\bar{\nu}_\tau$  curves of Fig. 3 are evident. The top antineutrino panel with pure  $\bar{\nu}_e$  injected is the simplest to understand. Below resonant energies, the vacuum angles are relevant, and we expect a flavor ratio of (5/9, 2/9, 2/9), as derived from Eq. (19) or equivalently from Eqs. (20) and (21). Above the resonant energies, the injected  $|\bar{\nu}_e\rangle$  is identified in matter with the state  $|1\rangle$ . In vacuum (e.g., at Earth) and to lowest order in  $\sin\theta_{13} \cos\delta$ , this mass state decomposes into the flavor ratio (2/3,  $(1 + 3\sqrt{2} \sin\theta_{13} \cos\delta)/6$ ,  $(1 - 3\sqrt{2} \sin\theta_{13} \cos\delta)/6$ ). At the  $3\text{-}\sigma$  maximal value of  $3\sqrt{2} \sin\theta_{13} \cos\delta = 0.90$ , the final  $\bar{\nu}_\tau$  fraction is driven almost to zero.

#### 4. (Anti)Neutrino flavors – inverted hierarchy

Next, we consider the inverted hierarchy, which is characterized by  $\delta m_{32}^2 < 0$ . Because the (decoherent) fluxes are unaffected by the mass hierarchy when  $\theta_{13} = 0$ , as discussed in Sec. II B 1, Fig. 2 remains valid for either mass hierarchy. In the more general situation with  $\theta_{13} \neq 0$ , it is no longer true that the  $|3\rangle$  eigenstate of the Hamiltonian completely decouples, and so a few additional considerations are necessary. First, note that only one of the two resonances occurs for neutrinos; the other one now appears in the antineutrino sector. In particular, the condition of a large resonance separation, which affects the quality of our approximation, is met trivially for the inverted hierarchy. Second, for the analysis of each resonance we can employ the same bases and approximations as we used for the normal hierarchy because the analysis essentially depends on the experimental result that  $|\delta m_{32}^2| \gg |\delta m_{21}^2|$  independent of the sign of  $\delta m_{32}^2$ .

Armed with these considerations, we find that the resonance between the states  $|1, r\rangle$  and  $|2, r\rangle$  stays in the neutrino sector, and the present results are equal to those in the lower-resonance normal-hierarchy situation. Hence, we only need to replace the superscripts  $l+ \rightarrow l-$  in Eqs. (50) and (52). This result is expected since the analysis

of the 1–2 resonance involves neither  $|3, r\rangle$  nor the value of  $\delta m_{32}^2$ . The resulting jump probability for neutrinos is

$$P_{kj} = \begin{pmatrix} 1 - P_c^l & P_c^l & 0 \\ P_c^l & 1 - P_c^l & 0 \\ 0 & 0 & 1 \end{pmatrix}, \quad (56)$$

where  $P_c$  is evaluated with Eqs. (46), (50), and the replacement  $l+ \rightarrow l-$ . Note that  $|1, r\rangle$  and  $|2, r\rangle$  are now the two heaviest states.

For antineutrinos, the resonance involves  $|1, r\rangle$  and  $|3, r\rangle$ , which are the two lightest states in the inverted mass hierarchy. An argument paralleling that leading to Eq. (53) yields for this case

$$\begin{aligned} E_R^{h-} &= -\frac{\delta m_{32}^2 + \delta m_{21}^2 \cos^2 \theta_{12}}{2V_e(0)} \cos 2\theta_{13}, \\ \tilde{E}_{NA}^{h-} &= \Gamma E = \pi \left| \frac{V_e}{V_e'} \right|_{r_R} (-\delta m_{32}^2 - \delta m_{21}^2 \cos^2 \theta_{12}), \\ \theta^{h-} &= \theta_{13}. \end{aligned} \quad (57)$$

Here, the superscript  $h-$  denotes the higher-energy inverted-hierarchy resonance. The energy for the onset of non-adiabaticity is given by

$$E_{NA}^{h-} = \frac{1}{3} \sin^2 \theta_{13} \tilde{E}_{NA}^{h-}, \quad (58)$$

and the jump-probability matrix now takes the form

$$P_{kj} = \begin{pmatrix} 1 - P_c^h & 0 & P_c^h \\ 0 & 1 & 0 \\ P_c^h & 0 & 1 - P_c^h \end{pmatrix}. \quad (59)$$

Here,  $P_c^h$  is determined by Eqs. (46) and (57). The inverted-hierarchy flavor fluxes on Earth for a representative set of neutrino parameters are shown in Fig. 4. A comparison of Figs. 3 and 4 reveals that the effect of moving the higher-energy resonance from the neutrino to the antineutrino sector via the change in mass hierarchy is dramatic.

The density-matrix formalism presented above accommodates any mixture of flavor fluxes produced in the solar core. For illustration, we have selected only examples with pure single-flavor initial states in Figs. 2, 3, and 4. The previously discussed sources are effectively incoherent, which implies that the fluxes for mixed-flavor cases can be inferred from these figures by simply taking the appropriately weighted incoherent sum of our pure-flavor results.

#### 5. Sensitivity to $\theta_{13}$

Because  $\theta_{13}$  is experimentally bounded to be less than about  $12^\circ$ , its measurement will be more difficult than that of the other two mixing angles. It is therefore interesting to discuss the  $\theta_{13}$  sensitivity of the terrestrial flavor ratios of neutrinos from solar WIMP annihilation.

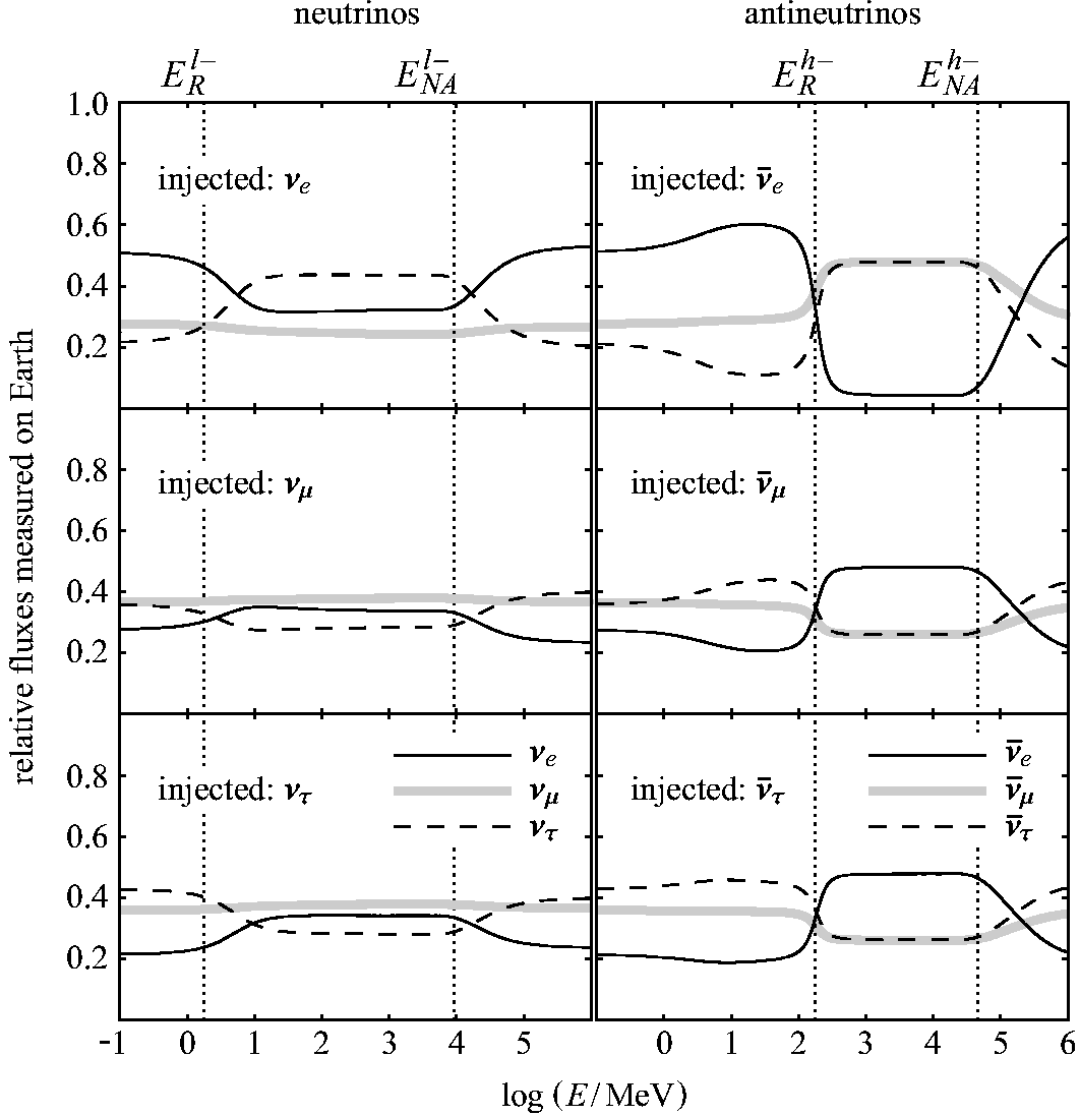


FIG. 4: Neutrino and antineutrino flavor probabilities on Earth versus energy, for the inverted hierarchy. Here, we have taken  $\delta m_{32}^2 = -3.0 \times 10^{-3} \text{ eV}^2$ . All other neutrino parameters are as in Fig. 3 (including  $\theta_{13} = 12^\circ$  and  $\delta = 0$ ). The  $\nu_\mu$  and  $\nu_\tau$  spectra and  $\bar{\nu}_\mu$  and  $\bar{\nu}_\tau$  spectra are interchanged if  $\delta = \pi$  is chosen.

Comparison of Fig. 2 with Figs. 3 and 4 reveals that the relative flavor fluxes on Earth indeed depend on  $\theta_{13}$ . The normal-hierarchy antineutrinos in Fig. 3 and the inverted-hierarchy neutrinos in Fig. 4 show changes with respect to Fig. 2 that are of the expected size  $\sin 12^\circ \sim 0.2$ . However, the changes for normal-hierarchy neutrinos and inverted-hierarchy antineutrinos are more significant. The question arises as to why a relatively small change in  $\theta_{13}$  can lead to effects of this magnitude.

The answer to this question lies in the transition from adiabaticity to non-adiabaticity for the higher resonance, which is governed by  $\theta_{13}$ : Equations (54) or (58) show that the onset of non-adiabaticity directly scales with  $\sin^2 \theta_{13}$ . In Fig. 2, we have taken  $\theta_{13} = 0$ . The loss of adiabaticity therefore occurs at zero energy. Moreover,

the level-crossing probability (46) becomes  $P_c^h = 1$  for zero mixing angle. In other words, the  $|3\rangle_m$  state is decoupled and does not participate in the adiabatic label permutation resulting from level repulsion, as discussed in Sec. II B 1. In Figs. 3 and 4, however,  $\theta_{13} \neq 0$  and  $|3\rangle_m$  is not decoupled. If in such a situation an adiabatic region exists—as in the case for  $\sin \theta_{13} = 12^\circ$ —the state experiences level permutation  $|3\rangle_m \rightarrow |2\rangle_m$  while propagating to the solar surface. It is this mechanism that causes the large  $\theta_{13}$  effects for normal-hierarchy neutrinos and inverted-hierarchy antineutrinos.

How small can  $\theta_{13}$  be for this effect to occur? Since the label permutation is valid only for energies above resonance in the adiabatic regime, we must require that  $E$  lies above the higher resonance and below the onset of



non-adiabaticity for this resonance, i.e.,

$$\begin{aligned} E_R^{h+} &< E < E_{NA}^{h+}, \\ E_R^{h-} &< E < E_{NA}^{h-}, \end{aligned} \quad (60)$$

for normal-hierarchy neutrinos and inverted-hierarchy antineutrinos, respectively. Here, the various energy scales are given by Eqs. (53), (54), (57), and (58). It follows that the onset of non-adiabaticity must lie above the resonance energy. Such will be the case for values of  $\theta_{13}$  down to a fraction of a degree.

We conclude that the terrestrial flavor fluxes from neutrinos originating in solar WIMP decay are quite sensitive to the mixing angle  $\theta_{13}$ . Accordingly, the study of solar-WIMP annihilation properties would greatly benefit from a pre-knowledge of the size of  $\theta_{13}$ . On the other hand, if dark-matter properties can be extracted from other experiments, such as direct WIMP discovery in underground detectors, or even better, at the LHC or ILC, then a measurement of  $\theta_{13}$  through WIMP annihilation in the Sun may be feasible.

## 6. The CP-violating phase $\delta$

Currently, the CP-violating phase  $\delta$  is unconstrained by experiments. We are thus led to study the effects of  $\delta$  on the propagation of high-energy solar neutrinos.

The general non-adiabatic density-matrix framework discussed in Sec. II C 2 has made no assumptions regarding the size of the phase  $\delta$ . The energy range of interest for solar neutrinos from WIMP decay is a few 100 MeV to about 100 GeV. Below this range, matter effects are suppressed and the standard vacuum results are approached. Above this range, absorption effects become dominant, and our framework is no longer accurate. Since this energy range is mainly below  $E_{NA}^{h\pm}$  and  $E_{NA}^{l\pm}$ , the adiabatic approximation is useful.

We again take  $\theta_{12}$  and  $\theta_{32}$  close to their observed tribimaximal values given in Sec. II A. For the remaining mixing angle, the largest experimentally allowed value  $\theta_{13} = 12^\circ$  is most interesting: From Eq. (9) one may infer that in a CP-conserving calculation, as here for decohered neutrino propagation, the  $\delta$  dependence will always occur in the combination  $\Re(e^{i\delta} \sin \theta_{13}) = \cos \delta \sin \theta_{13}$ . It is therefore only in combination with larger values of  $\theta_{13}$  that one may seek observable  $\delta$  effects. Thus, when illustrating effects of nonzero  $\delta$ , we will generally dramatize the result by taking  $\theta_{13}$  to be  $12^\circ$ , its maximally allowed  $3\text{-}\sigma$  value.

Concerning the  $\delta$ -parameter, two important analytic features emerge. The first is **Feature (i)**: *For  $\theta_{32} = 45^\circ$ , but arbitrary  $\theta_{21}$  and  $\theta_{13}$ , the replacement  $\delta \rightarrow \pi - \delta$  interchanges the role of  $\nu_\mu$  and  $\nu_\tau$ , and  $\bar{\nu}_\mu$  and  $\bar{\nu}_\tau$ , and leaves unaffected the terrestrial  $\nu_e$  and  $\bar{\nu}_e$  fluxes.* Although some versions of this result are known, we have included a proof in Appendix C for completeness. We remark that Feature (i) makes no assumptions about the neutrino energy

or adiabaticity, so that its validity actually extends beyond our energy range of interest, from a few 100 MeV to about 100 GeV.

Assuming continuity, Feature (i) implies that for  $\delta = 90^\circ$ , the  $\nu_\mu$  and  $\nu_\tau$  fluxes are identical. This is consistent with the previously determined condition  $\Re(U_{e3}) = 0$  for  $\nu_\mu$ - $\nu_\tau$  interchange symmetry: inspection of the mixing matrix  $U$  shows that  $U_{e3} = -i \sin \theta_{13}$  is purely imaginary for  $\delta = 90^\circ$ .

The second result is **Feature (ii)**: *For  $\theta_{32}$  and  $\theta_{12}$  at their tribimaximal values, the terrestrial flavor ratios for normal-hierarchy neutrinos and inverted-hierarchy antineutrinos are independent of  $\delta$  to zeroth order in  $(\delta m_{21}^2/\delta m_{32}^2)$ . In addition, the terrestrial  $\nu_e$  and  $\bar{\nu}_e$  fluxes are independent of  $\delta$  to zeroth order in  $(\delta m_{21}^2/\delta m_{32}^2)$  for any hierarchy.* This feature holds only in a finite energy region determined by adiabaticity and by  $V_e E \gg \delta m_{jk}^2$ . Fortunately, this energy region coincides with our range of interest, from a few 100 MeV to about 100 GeV; and fortunately again,  $(\delta m_{21}^2/\delta m_{32}^2) \sim 1/30$  is a small parameter. We verify this result in Appendix D.

As mentioned above,  $\theta_{13} = 0$  eliminates  $\delta$  from the mixing matrices  $U$  and  $U_m$ . It follows that Fig. 2, for instance, is unaffected by the value of  $\delta$ . Figures 3 and 4, on the other hand, should exhibit some changes when  $\delta$  is varied. With Features (i) and (ii) at hand, certain phase effects on the terrestrial flavor fluxes can be understood qualitatively. An immediate consequence of Features (i) and (ii) is the degeneracy of the  $\nu_\mu$  and  $\nu_\tau$  flavor spectra in the adiabatic region for normal-hierarchy neutrinos and inverted-hierarchy antineutrinos. This characteristic is apparent in Figs. 3 and 4. Feature (ii) implies that  $\delta$  effects are confined to the  $\bar{\nu}_\mu$  and  $\bar{\nu}_\tau$  fluxes in Fig. 3 and to the  $\nu_\mu$  and  $\nu_\tau$  fluxes in Fig. 4. We must look at these fluxes when seeking any sizable  $\delta$  dependence.

The qualitative behavior of these fluxes under changes of  $\delta$  is dictated by Feature (i). As  $\delta \rightarrow 90^\circ$ ,  $\delta$  and  $\pi - \delta$  approach each other, the  $\mu$ - and  $\tau$ -flavor fluxes must move toward each other; at  $\delta = 90^\circ$  they become degenerate. When  $\delta$  is increased further, the  $\mu$ - and  $\tau$ -flavor fluxes reverse their role with respect to each other. The first-order results for  $A_0$  in Appendix D establish that the  $\delta$  dependence of these fluxes is of the generic form  $B + C \sin \theta_{13} \cos \delta$ , where  $B$  and  $C$  depend on the mass hierarchy, on  $\nu$  versus  $\bar{\nu}$ , and on  $\theta_{13}$ . The precise expressions for  $B$  and  $C$  in each case can be inferred from Eqs. (D9) and (D13).

In Fig. 5, the  $\delta$  dependences of the various fluxes for inverted hierarchy (IH) neutrinos and normal hierarchy (NH) antineutrinos are shown. The NH neutrino and IH antineutrino spectra are not shown since their  $\cos \delta$  dependence is suppressed by the factor  $(\delta m_{21}^2/\delta m_{32}^2) \sim 1/30$ . Although the neutrino energy in the figure is taken to be  $E = 10$  GeV, the results remain approximately unchanged as long as  $E$  stays within our selected energy range. Apparent in Fig. 5 are the features discussed above. In particular, the  $\cos \delta \leftrightarrow -\cos \delta$  equivalence to the  $\mu \leftrightarrow \tau$  flavor interchange is evident.

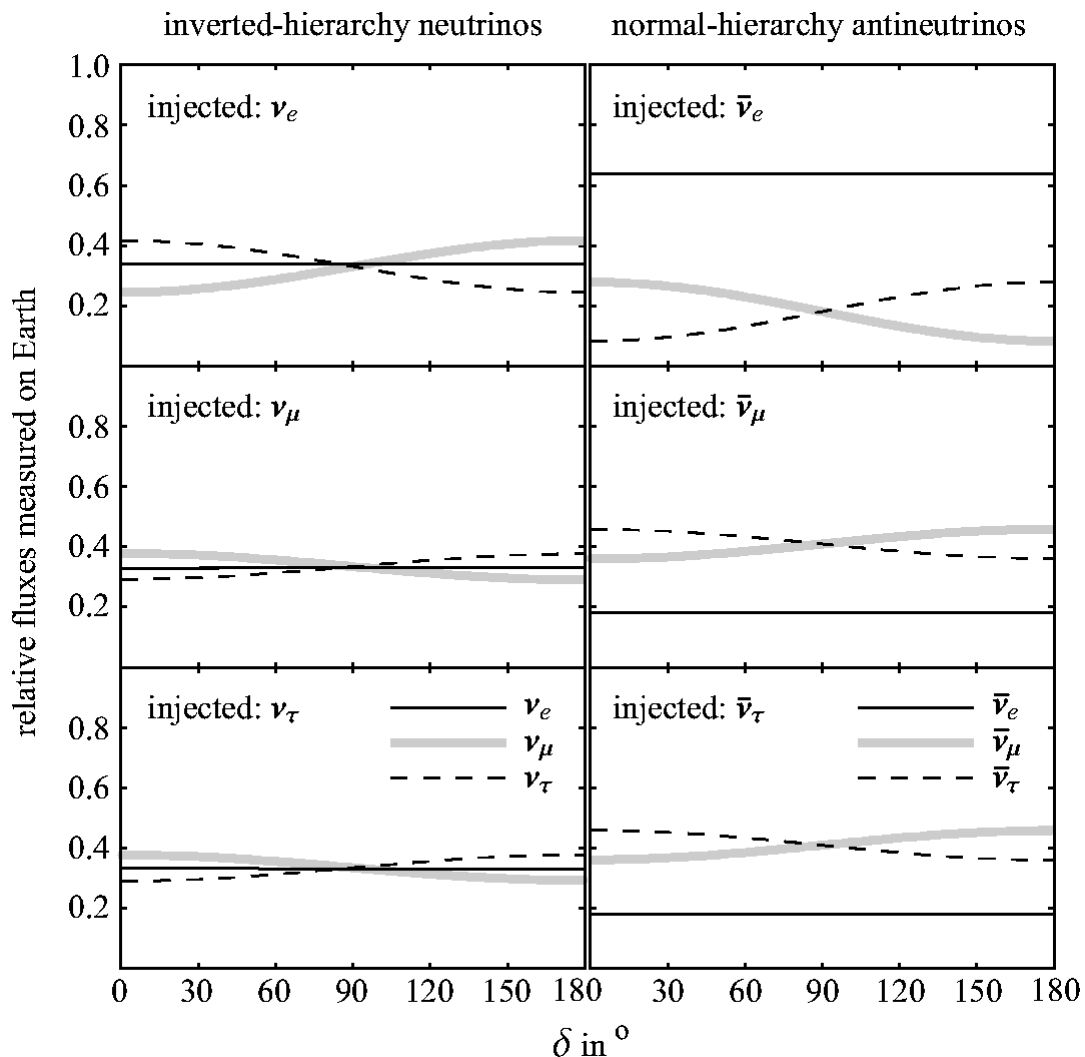


FIG. 5: Terrestrial neutrino fluxes versus the phase  $\delta$ . The neutrino mass-squared differences are  $\delta m_{21}^2 = 8.0 \times 10^{-5} \text{ eV}^2$  and  $\delta m_{32}^2 = \pm 3.0 \times 10^{-3} \text{ eV}^2$ , where the upper (lower) sign refers to the normal (inverted) hierarchy. The mixing angles are  $\theta_{12} = 35^\circ$ ,  $\theta_{13} = 12^\circ$ , and  $\theta_{23} = 45^\circ$ , and the neutrino energy is  $E = 10 \text{ GeV}$ . The  $\mu$ - and  $\tau$ -flavor fluxes exhibit opposite  $\cos \delta$  dependences, whereas the  $\nu_e$ -flavor fluxes are approximately constant. Curves for normal-hierarchy neutrinos and inverted-hierarchy antineutrinos are not shown, as they are all nearly constant as a function of  $\delta$ . These various results illustrate Features (i) and (ii) derived in the text.

### III. WIMP-MODEL PREDICTIONS FOR EARTHLY NEUTRINO FLAVORS

In general, the WIMP LSP is a superposition of four Majorana neutralino states. These are the two neutral Higgsinos (SUSY partners of the two Higgs doublets), the Bino (SUSY partner of the  $SU(2)$ -singlet  $B_\mu$  vector boson), and the neutral Wino (SUSY partner of the neutral  $W_\mu^0$  member of the  $SU(2)$ -triplet gauge boson). WMAP data yield  $\Omega_{\text{DM}} \simeq 23\%$ , which in turn constrains the decoupling of the WIMP and therefore bounds the WIMP mass and superposition. The non-observation of WIMPs in Tevatron data at Fermilab further constrains combinations of WIMP mass and superposition. However, the fact remains that almost any neutralino superposition

can be made consistent with present limits [34]. Theoretical arguments are largely expressions of preference or prejudice. For example, proponents of “gauge-mediated SUSY breaking” are led to a “Bino-like” LSP, while proponents of “anomaly-mediated SUSY breaking” are led instead to a “Wino-like” LSP. Thus, there is little guidance as to what neutralino superposition comprises the LSP.

Fortunately, two disjoint sets of annihilation channels are common in LSP models. One (I) is the  $W^+ W^-$  channel. The other (II) is the  $b\bar{b} + \tau^+ \tau^-$  channel. There are further channels available to WIMP annihilation beyond (I) and (II), but these are calculated to be subdominant. Higgsino and Wino annihilation favor channel I, if the LSP mass exceeds  $M_W$ ; Higgsino annihilation but not

Wino annihilation also produces  $ZZ$  if above threshold, but the neutrino spectrum resulting from this channel is similar to that from  $W^+W^-$ , so we need not consider  $ZZ$  separately. Bino annihilation favors channel II, although even a small amount of mixing of the Bino with other neutralinos is likely to lead to a dominance of  $W^+W^-$  production. For an LSP with mass less than  $M_W$ , the decay channel of the LSP is (II).

Since the annihilating WIMPs are a CP-symmetric initial state, the neutrino and antineutrino spectra emerging from WIMP annihilation must be identical. The flavor processing by solar matter, described in this work, is not CP-symmetric. Therefore, differences between neutrino and antineutrino flavor ratios at Earth are expected. Conversely, any observed differences between neutrino and antineutrino flavor ratios at Earth are an indication of the solar matter effect. In principle, it is possible to separate neutrino and antineutrino spectra in proposed, large, magnetized iron-calorimeter experiments.

It is not hard to understand the reasons for the two preferred decay channels. Pairs of  $SU(2)$ -doublet Higgsinos or Winos have an electroweak coupling to  $W^+W^-$  suppressed only by the  $t$ -channel  $\tilde{W}$  exchange. However, the  $SU(2)$ -singlet Bino does not have this coupling. On the other hand, when the  $W^+W^-$  channel is not available, all LSP pairs, being Majorana particles, annihilate to massless final-state pairs in an  $l = 1$  ( $p$ -wave) angular-momentum state suppressed by  $\beta_{\text{DM}}^3$ , where  $\beta_{\text{DM}}$  is the velocity of the LSP. With massive final-state pairs, chirality flips enable an  $s$ -wave decay suppressed by the factor  $\beta_{\text{DM}}(m_{\text{final}}^2/M_{\text{DM}}^2)$ . The velocity of the non-relativistic LSPs is sufficiently small that the  $s$ -wave dominates and one gets the  $b\bar{b}$  final state  $N_C m_b^2/(N_C m_b^2 + m_\tau^2) = 95\%$  of the time, and the  $\tau^+\tau^-$  final state  $m_\tau^2/(N_C m_b^2 + m_\tau^2) = 5\%$  of the time; here,  $N_C = 3$  is the number of QCD colors. The neutrinos from tau decay  $\tau \rightarrow \nu_\tau + \dots$  are more copious and provide a harder spectrum than those from  $b$  decay, so it turns out that the 5%  $\tau^+\tau^-$  mode makes a significant contribution to the final neutrino flux.

In the figures to follow, in which all  $w_\alpha$  are taken from Ref. [18], we will display the flavor ratios to be expected at Earth for the two WIMP annihilation classes (I) and (II). For further insight, we will also show separately results for the pure  $b\bar{b}$  and pure  $\tau^+\tau^-$  decay modes. However, before displaying the flavor ratios expected at Earth, we show in Fig. 6 the flavor ratios produced by WIMP annihilation in the Sun for each of the four decay modes. These flavor spectra are qualitatively easy to understand. The  $b\bar{b}$  production and subsequent decay to (charm+)  $\tau + \nu_\tau$  is phase-space suppressed relative to decay to (charm+)  $e + \nu_e$  or  $\mu + \nu_\mu$ , particularly so when the neutrino is produced at higher energy. In  $\tau^+\tau^-$  production and decay, the branching ratio to  $\nu_\tau$  is unity, but there are also 17% branching ratios to  $\nu_e$  and to  $\nu_\mu$ . Accompanying the  $\nu_\mu$  is a muon, which will itself decay to produce another  $\nu_\mu$  and  $\nu_e$ , but at much lower energy since the muon loses considerable energy in the Sun's

magnetic field before decaying. So roughly, the flavor ratios from the  $\tau^+\tau^-$  mode are  $(1.0 : 0.17 : 0.17)/1.34$ . In  $W^+W^-$  production and decays, neutrinos at high energies are democratically produced, and the associated taus and muons quickly lose energy in the Sun's center. However, at lower energy, the neutrino flux originates from the decay of nearly-stopped heavy quarks produced in  $W$  fragmentation, so there is a low-energy depletion of  $\nu_\tau$ s.

A useful summary of Fig. 6 is that, at production in the Sun, (i) the flavor fluxes are the same for neutrino and antineutrino, and (ii) the  $e$  and  $\mu$  flavors are produced in equal amounts, but the amount of  $\tau$  flavor depends on the WIMP annihilation channel. In the  $b\bar{b}$  channel,  $\tau$  is suppressed relative to  $e$  and  $\mu$ , especially at higher energies. In the  $\tau^+\tau^-$  channel, it is just the opposite, with the  $\tau$ -flavor contribution enhanced, especially at higher energies. The implication for the realistic channel (II) consisting of 95%  $b\bar{b} + 5\% \tau^+\tau^-$  is a suppressed  $\tau$  component at lower energies, and a highly enhanced  $\tau$  component at higher energies. For the realistic  $W^+W^-$  channel (I), the  $\tau$  component is negligible below about 20 GeV, whereas  $\tau$ ,  $e$ , and  $\mu$  are equally represented above 20 GeV. It was claimed in Sec. II C 2 that a democratic 1 : 1 : 1 flavor ratio at production necessarily implies a democratic flavor ratio at Earth. Thus, we expect flavor democracy at Earth for neutrino energies above  $\sim 20$  GeV, if the WIMP annihilation mode in the Sun is dominantly  $W^+W^-$ . Figures to be shown will bear this out. For all other channels, and for the  $W^+W^-$  channel below 20 GeV, the flavors at production are far from democratic, and the flavor-evolution machinery developed in this work is important.

The solar flavor spectra of Fig. 6 get processed by the physics we have derived in this paper. The resulting flavor spectra at Earth are shown in Figs. 7–10 for the  $b\bar{b}$ ,  $\tau^+\tau^-$ , 95%  $b\bar{b} + 5\% \tau^+\tau^-$ , and  $W^+W^-$  WIMP-annihilation channels, respectively. For each of the three sample WIMP masses  $m_{\text{DM}} = 10, 30, \text{ and } 100$  GeV, the three values  $\theta_{13} = 0^\circ, 1^\circ, \text{ and } 12^\circ$  are considered. We have further taken  $\delta = 0$ , which serves to maximize  $|\sin\theta_{13} \cos\delta|$  and therefore the sensitivity to  $\theta_{13}$ . Results are displayed for the normal and the inverted mass hierarchies.

The greater likelihood of the (I)  $W^+W^-$  and (II) 95%  $b\bar{b} + 5\% \tau^+\tau^-$  decay channels directs our attention to Figs. 9 and 10. In Fig. 10 one sees the 1 : 1 : 1 flavor ratio at Earth for energies above 20 GeV, that results from the democratic production ratio in the Sun at these energies for the  $W^+W^-$  channel. Below 20 GeV in the  $W^+W^-$  channel, and for the whole energy range in the 95%  $b\bar{b} + 5\% \tau^+\tau^-$  channel, a comparison of Figs. 9 and 10 to Fig. 6 makes the point that significant flavor processing occurs as neutrinos propagate outward through the Sun. The flavor processing tends to homogenize the  $\mu$  and  $\tau$  components. Nevertheless, in the lower energy region of (I) and higher energy region of (II), the flavor ratios differ significantly from unity.

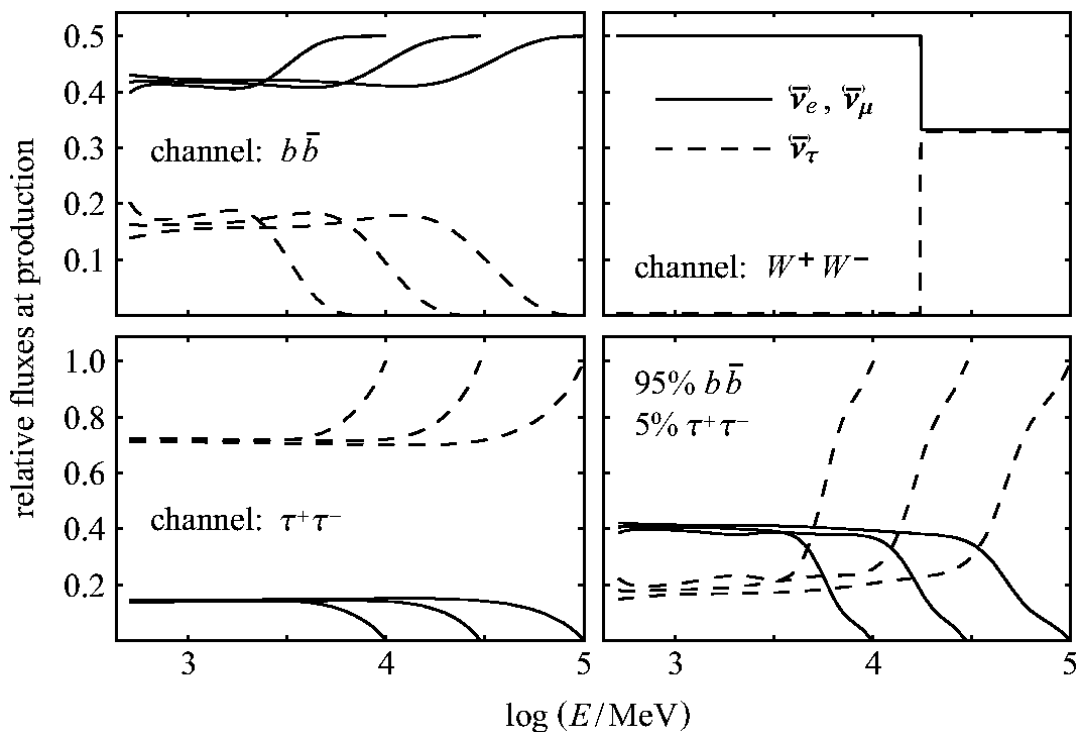


FIG. 6: Relative (anti)neutrino flavor fluxes at production in the solar core are plotted versus neutrino energy  $E$  for four scenarios: dark-matter annihilation predominantly into  $b\bar{b}$ , or predominantly into  $W^+W^-$ , or predominantly into  $\tau^+\tau^-$ , or predominantly into 95%  $b\bar{b}$  + 5%  $\tau^+\tau^-$ . Solid (dashed) lines display the  $e$  and  $\mu$  ( $\tau$ ) flavor fluxes. For each scenario, dark-matter masses  $m_{\text{DM}}$  of 10 GeV, 30 GeV, and 100 GeV have been considered. The dark-matter mass can be inferred from the threshold energies of the graphs. This plot was generated from the results in Ref. [18].

Comparison of Figs. 9 and 10 makes the further point that flavor ratios arriving at Earth do vary with the WIMP decay channel. In fact, for the favored channels (I) and (II), flavor signatures are usefully in opposition, in that the  $W^+W^-$  channel offers democratic flavors at higher energies and not at lower energies, whereas the 95%  $b\bar{b}$  + 5%  $\tau^+\tau^-$  channel offers nearly democratic flavors at lower energies and not at higher energies. For the  $W^+W^-$  channel, the change from non-democratic to democratic is fixed at  $\sim 20$  GeV, a number traceable to Standard Model masses. For the 95%  $b\bar{b}$  + 5%  $\tau^+\tau^-$  channel, the energy for change from nearly democratic to non-democratic depends on the WIMP mass. For either channel, flavor ratios in the non-democratic regions are seen to depend on  $\theta_{13}$ , and, for  $\theta_{13} \neq 0$ , on the mass hierarchy. For the 95%  $b\bar{b}$  + 5%  $\tau^+\tau^-$  channel, certain flavor ratios may be as large as 2 at the higher energies; and in the  $W^+W^-$  channel, as large as 1.4 below  $\sim 20$  GeV. The flavor ratio of 2 is within experimental reach, while ratios of 1.4 or smaller may present a challenge for some neutrino telescopes [21] but perhaps not for others [22].

#### IV. SUMMARY AND CONCLUSIONS

The discovery of  $\gtrsim$  GeV neutrinos from the Sun would constitute strong evidence for the annihilation of solar

WIMPs. Competing WIMP models can in principle be distinguished by the energy spectrum and flavor ratios of the decay neutrinos and antineutrinos. The flavor ratios detected at Earth will differ from the flavor ratios at injection in the Sun's core. Due to the decoherence resulting from  $\langle L/E \rangle$ -averaging in the Sun, the flavor evolution is described by classical probabilities, rather than by quantum-mechanical amplitudes. This simplifies the analysis. On the other hand, the evolution is complicated by the matter effects within the Sun. WIMPs annihilate in a CP-symmetric state, and so the neutrino and antineutrino spectra at the point of origin are identical in energies and flavors. However, since the material of the Sun is matter and not antimatter, propagation effects through the Sun are different for neutrino versus antineutrino. In the travel outward from the Sun's core, two level-crossings are encountered (one if  $\theta_{13} = 0$ ), each described by an MSW resonance. For the normal neutrino-mass hierarchy, both level crossings occur in the neutrino sector; whereas for the inverted hierarchy, the lower-energy crossing occurs in the neutrino sector and the higher-energy resonance occurs in the antineutrino sector. Thus, the emergent energy and flavor spectra depend also on the neutrino-mass hierarchy, as indicated schematically in Fig. 1. An additional complication is that evolution at the level crossings may be adiabatic or non-adiabatic, depending on solar and neutrino parame-

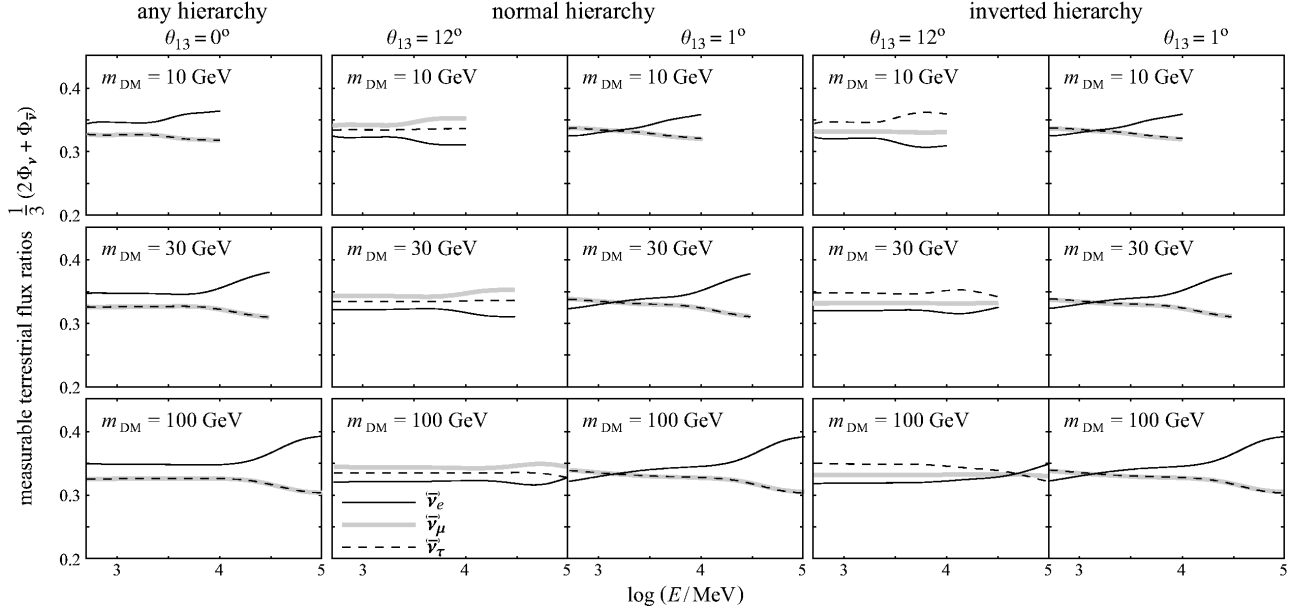


FIG. 7: Terrestrial fluxes versus neutrino energy  $E$  for solar WIMP annihilation predominantly into  $b\bar{b}$ . The quantity  $(2\Phi_\nu + \Phi_{\bar{\nu}})/3$  is plotted, where the  $\nu$  and  $\bar{\nu}$  fluxes are weighted according to their cross sections for detection. This quantity would be measured by Earth-based detectors that cannot resolve  $\nu_\alpha$  from  $\bar{\nu}_\alpha$  events, as discussed in Sec. II B 5. The neutrino mass-squared differences are  $\delta m_{21}^2 = 8.0 \times 10^{-5} \text{ eV}^2$  and  $\delta m_{32}^2 = \pm 3.0 \times 10^{-3} \text{ eV}^2$ . The mixing angles are  $\theta_{12} = 35^\circ$  and  $\theta_{23} = 45^\circ$ , and the CP-violating phase  $\delta$  has been set to zero. We have considered the values  $\theta_{13} = 0^\circ, 1^\circ, \text{ and } 12^\circ$  for each hierarchy and for each of the dark-matter masses  $m_{\text{DM}} = 10 \text{ GeV}, 30 \text{ GeV}, \text{ and } 100 \text{ GeV}$  (from top to bottom). The  $\nu_\mu$  and  $\nu_\tau$  spectra as well as the  $\bar{\nu}_\mu$  and  $\bar{\nu}_\tau$  spectra are interchanged if  $\delta = \pi$  is chosen. Note that the observables depend noticeably on the mixing angle  $\theta_{13}$ . Moreover, for larger  $\theta_{13}$  angles there are visible differences between the normal and inverted hierarchies.

ters.

In this work, we presented analytic formulas for the complete flavor evolution. One virtue of an analytic treatment is the emergence of *post hoc* intuition. With the gift of hindsight, we therefore were able to present the physics of flavor evolution which underlies the analytic formulas. For example, we were able to derive general statements that

- (i) If flavor democracy, defined by 1 : 1 : 1 flavor ratios, occurs in WIMP decay, then the same 1 : 1 : 1 ratio must be observed on Earth; in other words, flavor-mixing, even with complicated matter effects, cannot derail democracy!
- (ii) For maximal  $\theta_{32}$  but arbitrary  $\theta_{21}$  and  $\theta_{13}$ , the replacement  $\delta \rightarrow \pi - \delta$  interchanges the role of  $\nu_\mu$  and  $\nu_\tau$ , and  $\bar{\nu}_\mu$  and  $\bar{\nu}_\tau$ , and leaves unaffected the terrestrial  $\nu_e$  and  $\bar{\nu}_e$  fluxes.
- (iii) For  $\theta_{32}$  and  $\theta_{12}$  at their tribimaximal values, the terrestrial flavor ratios for normal-hierarchy neutrinos and inverted-hierarchy antineutrinos are independent of  $\delta$  to zeroth order in  $(\delta m_{21}^2/\delta m_{32}^2)$ . In addition, the terrestrial  $\nu_e$  and  $\bar{\nu}_e$  fluxes are independent of  $\delta$  to zeroth order in  $(\delta m_{21}^2/\delta m_{32}^2)$  for any hierarchy. (This feature holds only in a finite energy region determined by adiabaticity and by  $V_e E \gg \delta m_{jk}^2$ .)

Concerning the adiabaticity versus non-adiabaticity, we found that level-crossings are adiabatic in the neu-

trino sector for energies up to  $\sim 10 \text{ GeV}$  or more in the neutrino sector. In the antineutrino sector, there are no level crossings for the normal hierarchy and so adiabaticity holds trivially at all energies, while for the inverted hierarchy, adiabaticity holds up to  $\sim 50 \text{ GeV}$  or more. The energy-onsets of non-adiabatic behavior ( $E_{NA}$ ) are indicated in Figs. 2-4.

There is a striking dependence on the value of the unknown mixing-angle  $\theta_{13}$  in the evolution of flavor away from a single injected flavor in the Sun. In particular, the limit  $\theta_{13} \rightarrow 0$  is “discontinuous” in that for  $\theta_{13} = 0$  the third neutrino mass eigenstate  $|3\rangle$  is completely decoupled from the other two mass eigenstates, and there is but a single resonance is encountered in the flavor evolution; while for  $\theta_{13} \neq 0$ , two resonances are encountered, and even a small nonzero value of  $\theta_{13}$  may be amplified by the associated resonance. In addition, for nonzero  $\theta_{13}$ , there is sensitivity to the CP- and T-symmetric term  $\sin\theta_{13} \cos\delta$ , where  $\delta$  is the CP- and T-violating phase parameter in the unitary mixing-matrix. Flavor evolution from a single injected flavor in the Sun, for  $\theta_{13}$  set to zero, is shown in Fig. 2. For the maximal allowed value of  $\theta_{13}$ , the same is shown in Fig. 3 for the normal mass-hierarchy, and in Fig. 4 for the inverted hierarchy.

We further explored the dependence on  $\delta$  in Fig. 5. The dependence on  $\delta$  enters through the CP- and T-even factor  $\Re\{U_{e3}\} = \sin\theta_{13} \cos\delta$ . To maximize sensitivity to  $\delta$  in this figure, we have again chosen for  $\theta_{13}$  the max-

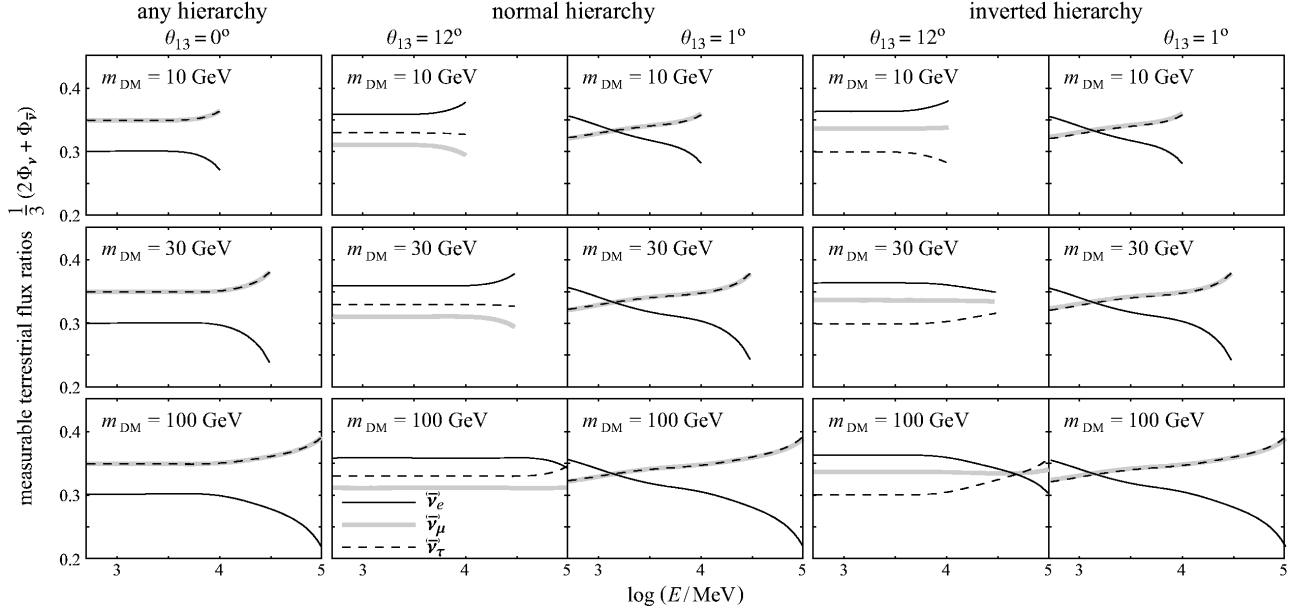


FIG. 8: Terrestrial fluxes versus neutrino energy  $E$  for solar WIMP annihilation predominantly into  $\tau^+\tau^-$ . Again, the observable  $(2\Phi_\nu + \Phi_{\bar{\nu}})/3$  is plotted. Neutrino parameters are identical to those employed in Fig. 7. The  $\nu_\mu$  and  $\nu_\tau$  spectra as well as the  $\bar{\nu}_\mu$  and  $\bar{\nu}_\tau$  spectra are interchanged if  $\delta = \pi$  is chosen. Sensitivities to  $\theta_{13}$  and the mass hierarchy occur at levels similar to those of the  $b\bar{b}$  case in Fig. 7.

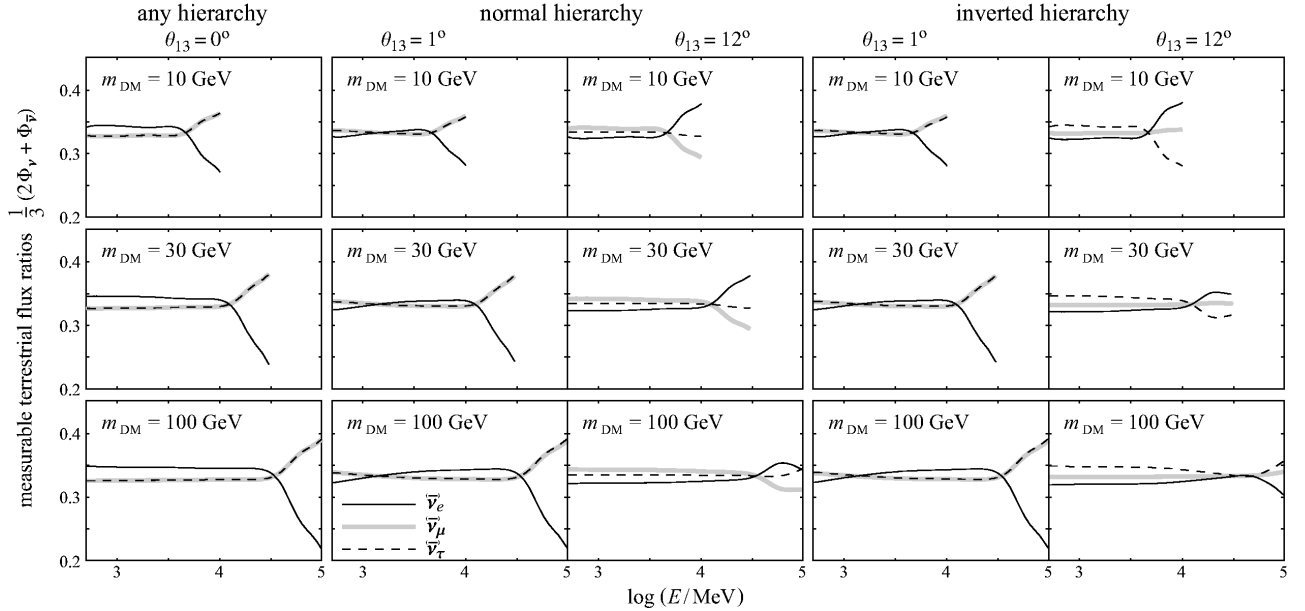


FIG. 9: Terrestrial fluxes versus neutrino energy  $E$  for solar WIMP annihilation into  $95\% b\bar{b} + 5\% \tau^+\tau^-$ . Again the observable  $(2\Phi_\nu + \Phi_{\bar{\nu}})/3$  is plotted, and neutrino parameters are identical to those in Figs. 7 and 8. The  $\nu_\mu$  and  $\nu_\tau$  spectra as well as the  $\bar{\nu}_\mu$  and  $\bar{\nu}_\tau$  spectra are interchanged if  $\delta = \pi$  is chosen. Sensitivities to  $\theta_{13}$  and the mass hierarchy are comparable to those in Figs. 7 and 8, as expected.

imum value allowed by the CHOOZ data,  $12^\circ$ . The  $\mu$  and  $\tau$  flavored spectra are sensitive to  $\delta$ , whereas the  $e$  spectrum is not. The  $\nu_\mu$  and  $\nu_\tau$  spectra and the  $\bar{\nu}_\mu$  and  $\bar{\nu}_\tau$  spectra swap among themselves for  $\delta \rightarrow \pi - \delta$ . These results are in accord with the general features mentioned

above.

WIMP decay does not produce neutrinos of just one flavor. Consequently, our illustrative evolution results in Figs. 2-5 do not apply directly to the flavor processing of WIMP-decay neutrinos. Rather, some linear com-

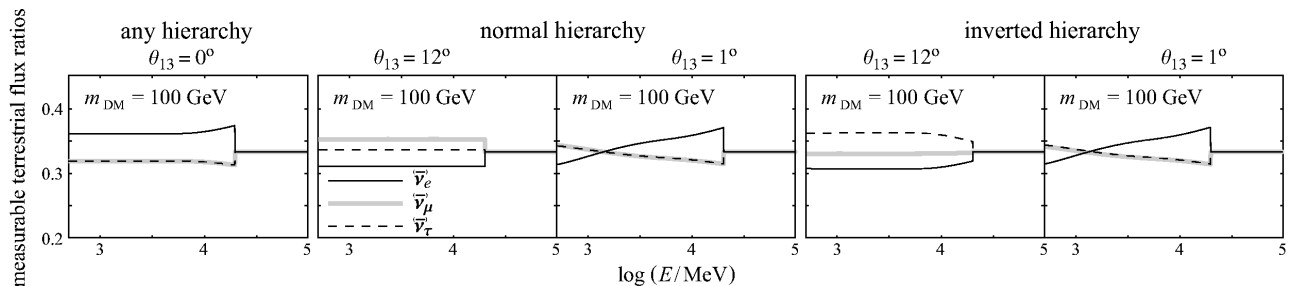


FIG. 10: Terrestrial fluxes versus neutrino energy  $E$  for WIMP annihilation predominantly into  $W^+W^-$ . The plotted observable  $(2\Phi_\nu + \Phi_{\bar{\nu}})/3$  and the neutrino parameters are the same as those in Figs. 7–9. The  $\nu_\mu$  and  $\nu_\tau$  spectra as well as the  $\bar{\nu}_\mu$  and  $\bar{\nu}_\tau$  spectra are interchanged if  $\delta = \pi$  is chosen. Sensitivities to  $\theta_{13}$  and the mass hierarchy are comparable to those in Figs. 7–9.

binations of the single-flavor figures are relevant. In most WIMP models, the annihilation final states fall into one of two categories. The two are the  $W^+W^-$  final state and the 95%  $b\bar{b} + 5\% \tau^+\tau^-$  final state. These Standard Model final states decay further in well known ways to produce the neutrinos and antineutrinos emanating from the Sun’s core. In Fig. 6 we showed the injection neutrino and antineutrino spectra per flavor, gleaned from [18]. A representative sample of WIMP masses were chosen: 10 GeV, 30 GeV, and 100 GeV. The flavor spectra arriving at Earth, after mixing and matter processing, we showed in Figs. 7-10 for various possible WIMP-annihilation final states. Each of these Figures is arranged into panels labeled by the three values  $\theta_{13} = 0^\circ, 1^\circ, 12^\circ$ , and the three values of WIMP mass 10 GeV, 30 GeV, 100 GeV. The phase  $\delta$  has been set to zero (or  $\delta = \pi$  with the interchange of  $\nu_\mu$  and  $\nu_\tau$  spectra and  $\bar{\nu}_\mu$  and  $\bar{\nu}_\tau$  spectra); we reserve for future work the dependence of the observable flavor spectra on  $\delta$  [35]. One feature of the flavor evolution is a tendency to average the  $\mu$  and  $\tau$  flavors. Nevertheless, some interesting nontrivial flavor ratios appear in these figures.

For the two preferred channels of WIMP annihilation, it is seen that in the lower energy region of the  $W^+W^-$  decay mode, and in the higher energy region of the 95%  $b\bar{b} + 5\% \tau^+\tau^-$  decay mode, flavor ratios differ significantly from unity. Conversely, in the higher and lower energy regions, respectively, the flavor ratios are (nearly) democratic. Since the decay mode implicates the nature of the WIMP, the experimental ability to distinguish decay modes allows an inference of the nature of the WIMP. The energy dependences of the neutrino flavor ratios at Earth are, then, the signatures which potentially distinguish the two main competing WIMP models.

The flavor ratios at Earth depend on  $\theta_{13}$  and on the neutrino mass hierarchy. For the purpose of studying the nature of solar WIMPS, it would be very useful if near future experiments would better determine these two parameters. On the other hand, if the nature of the WIMP becomes known from future accelerators such as the LHC and/or the ILC, then it becomes conceivable to use the flavor ratios to deduce or bound better  $\theta_{13}$ , and possibly deduce the mass hierarchy.

If one attempts either to infer the nature of the solar WIMP, or to determine the values of the parameters  $\theta_{13}$  and  $\text{sign}(\delta m_{32}^2)$ , an algorithm for neutrino flavor processing from the Sun’s core outward is essential. In this paper, we have provided this algorithm.

### Acknowledgments

We gratefully acknowledge informative conversations with Dan Hooper and Xerxes Tata. This work was supported in part by the DOE under cooperative research agreement No. DE-FG02-05ER41360 and under Grant No. DE-FG05-85ER40226. RL acknowledges support by the European Commission under Grant No. MOIF-CT-2005-008687, and TW thanks Manfred Lindner for hospitality and support at MPI-Heidelberg during the final stage of paper preparation.

### APPENDIX A: ANALYTIC $U_m$ FOR NONZERO $\theta_{13}$ AND $\delta$

In order to obtain a manageable expression for  $U_m$ , we restrict our attention primarily to perturbations about the tribimaximal case (10). In particular, we take  $\theta_{12} = \pi/6 + \delta\theta_{12}$ , and we implicitly assume  $\tan\theta_{13} \lesssim \mathcal{O}(1)$ , which is observationally justified. On phenomenological grounds, we also have  $\delta m_{21}^2/\delta m_{32}^2 \ll 1$  and  $\delta m_{jk}^2/V_e(0)E \ll 1$ , so that these quantities can serve as additional expansion parameters. In the latter relation, we have employed the fact that our present focus is on GeV neutrinos.

We begin by recalling the defining relation for  $U_m$ :

$$H_M = U_m^\dagger \left[ U \hat{M} U^\dagger + \hat{V} \right] U_m, \quad (\text{A1})$$

such that  $H_M$  is diagonal. For notational brevity we have defined  $\hat{M} = \text{diag}(-\delta m_{21}^2, 0, \delta m_{32}^2)/2E$  (as before), and  $\hat{V} = V_e \text{diag}(1, 0, 0)$ . In order to simplify the algebra, we decompose  $U_m$  as follows:

$$U_m = R_{23}(\theta_{23}) U_\delta^\dagger \tilde{U}_m, \quad (\text{A2})$$

with  $\tilde{U}_m$  to be determined. Employing this decomposition and Eq. (7) in the definition (A1) we obtain

$$H_M(\delta) = \tilde{U}_m^\dagger \left[ R_{13} U_\delta R_{12} \hat{M} R_{12}^\dagger U_\delta^\dagger R_{13}^\dagger + \hat{V} \right] \tilde{U}_m. \quad (\text{A3})$$

Here, we have suppressed the arguments of the rotation matrices, and we have used that both  $R_{23}$  and  $U_\delta$  commute with  $\hat{V}$ . Since  $\tilde{U}_m$  is unitary and diagonalizes  $R_{13} U_\delta R_{12} \hat{M} R_{12}^\dagger U_\delta^\dagger R_{13}^\dagger + \hat{V} \equiv \tilde{H}$ , it is composed of normalized eigenvectors of  $\tilde{H}$ . To find these, we can employ perturbation theory: we have  $\delta m_{jk}^2 \ll EV_e$ , so that  $R_{13} U_\delta R_{12} \hat{M} R_{12}^\dagger U_\delta^\dagger R_{13}^\dagger \equiv \delta \tilde{H}$  can be treated as a perturbation when compared to  $\hat{V}$ .

The first step in time-independent perturbation theory is to identify the zeroth-order eigenstates, which in the present situation are those of  $\hat{V}$ . Up to a phase, the first such eigenvector clearly is

$$v_1 = (1, 0, 0). \quad (\text{A4})$$

The remaining two eigenvectors  $v_2$  and  $v_3$ , which are a linear combination of  $(0, 1, 0)$  and  $(0, 0, 1)$ , are associated with degenerate eigenvalues. They must therefore be determined by diagonalizing  $\delta \tilde{H}$  restricted to the 2–3 subspace. This essentially amounts to finding the eigenvectors of the lower right  $2 \times 2$  block of

$$\begin{aligned} \delta \tilde{H} = & \frac{1}{12E} \begin{pmatrix} 6\delta m_{32}^2 \sin^2 \theta_{13} - 4\delta m_{21}^2 \cos^2 \theta_{13} & 2\sqrt{2} e^{i\delta/2} \delta m_{21}^2 \cos \theta_{13} & (2\delta m_{21}^2 + 3\delta m_{32}^2) \sin 2\theta_{13} \\ 2\sqrt{2} e^{-i\delta/2} \delta m_{21}^2 \cos \theta_{13} & -2\delta m_{21}^2 & -2\sqrt{2} e^{-i\delta/2} \delta m_{21}^2 \sin \theta_{13} \\ (2\delta m_{21}^2 + 3\delta m_{32}^2) \sin 2\theta_{13} & -2\sqrt{2} e^{i\delta/2} \delta m_{21}^2 \sin \theta_{13} & 6\delta m_{32}^2 \cos^2 \theta_{13} - 4\delta m_{21}^2 \sin^2 \theta_{13} \end{pmatrix} \\ & + \frac{\delta m_{21}^2}{6E} \begin{pmatrix} 2\sqrt{2} \cos^2 \theta_{13} & e^{i\delta/2} \cos \theta_{13} & -\sqrt{2} \sin 2\theta_{13} \\ e^{-i\delta/2} \cos \theta_{13} & -2\sqrt{2} & -e^{-i\delta/2} \sin \theta_{13} \\ -\sqrt{2} \sin 2\theta_{13} & -e^{i\delta/2} \sin \theta_{13} & 2\sqrt{2} \sin^2 \theta_{13} \end{pmatrix} \delta \theta_{12}. \end{aligned} \quad (\text{A5})$$

Here,  $\delta \theta_{12}$  denotes deviations of  $\theta_{12}$  from its tribimaximal value implicitly determined by  $\sin^2 \theta_{12} = 1/3$ . The above expression (A5) is valid at first order in  $\delta \theta_{12}$ . We remark that the correction term involving  $\delta \theta_{12}$  contains  $\delta m_{21}^2$  as an overall factor, but  $\delta m_{32}^2$  is absent in the  $\delta \theta_{12}$  term. This essentially arises because in the definition of  $\delta \tilde{H}$  the  $R_{12}$  matrix mixes only the upper  $2 \times 2$  block of  $\hat{M}$ , so that any occurrence of  $\theta_{12}$  is necessarily accompanied by a  $\delta m_{21}^2$  factor.

For the remaining zeroth-order eigenvectors, we now find at leading order in  $\delta m_{21}^2/\delta m_{32}^2$

$$v_2 = \begin{pmatrix} 0 \\ e^{-i\delta/2} \\ \frac{\sqrt{2}}{3} \frac{\tan \theta_{13}}{\cos \theta_{13}} \frac{\delta m_{21}^2}{\delta m_{32}^2} \end{pmatrix}, \quad (\text{A6})$$

and

$$v_3 = \begin{pmatrix} 0 \\ -\frac{\sqrt{2}}{3} \frac{\tan \theta_{13}}{\cos \theta_{13}} \frac{\delta m_{21}^2}{\delta m_{32}^2} e^{-i\delta/2} \\ 1 \end{pmatrix}. \quad (\text{A7})$$

We remind the reader that normalized eigenvectors are only defined up to phases. Note that these expressions are independent of  $\delta \theta_{12}$ . This is a consequence of the fact that  $\delta m_{32}^2$  is absent in the  $\delta \theta_{12}$  term in Eq. (A5), so that the  $\delta \theta_{12}$  correction contains a further suppression relative to the  $\delta \theta_{12}$ -independent contribution in  $\delta \tilde{H}$ .

The corrections to these eigenvectors are given by the usual perturbation-theory formula

$$\delta v_j = \sum_k \frac{v_k^\dagger \delta \tilde{H} v_j}{\lambda_j - \lambda_k} v_k, \quad (\text{A8})$$

where  $\lambda_j$  denotes the eigenvalue of  $\hat{V}$  corresponding to  $v_j$ , i.e.,  $\lambda_1 = V_e$  and  $\lambda_2 = \lambda_3 = 0$ . The sum in Eq. (A8) runs over all eigenvectors that do not belong to the eigenspace containing  $v_j$ . We obtain

$$\begin{aligned} \delta v_1 &= \frac{1}{V_e E} \begin{pmatrix} 0 \\ \frac{1}{3\sqrt{2}} e^{-i\delta/2} \delta m_{21}^2 \cos \theta_{13} \\ \frac{1}{12} (3\delta m_{32}^2 + 2\delta m_{21}^2) \sin 2\theta_{13} \end{pmatrix}, \\ \delta v_2 &= \frac{1}{V_e E} \begin{pmatrix} -\frac{1}{3\sqrt{2}} \delta m_{21}^2 \cos \theta_{13} \\ 0 \\ 0 \end{pmatrix}, \\ \delta v_3 &= \frac{1}{V_e E} \begin{pmatrix} -\frac{1}{12} (3\delta m_{32}^2 + 2\delta m_{21}^2) \sin 2\theta_{13} \\ 0 \\ 0 \end{pmatrix}, \end{aligned} \quad (\text{A9})$$

at leading order in  $\delta m_{21}^2/\delta m_{32}^2$ . It follows that our approximation  $\tilde{U}_m \simeq (v_1 + \delta v_1, v_2 + \delta v_2, v_3 + \delta v_3)$  is explicitly given by



$$\tilde{U}_m = \begin{pmatrix} 1 & -\frac{\delta m_{21}^2 \cos \theta_{13}}{3\sqrt{2}V_e E} & -\frac{(2\delta m_{21}^2 + 3\delta m_{32}^2) \sin 2\theta_{13}}{12V_e E} \\ \frac{\delta m_{21}^2 e^{-i\delta/2} \cos \theta_{13}}{3\sqrt{2}V_e E} & e^{-i\delta/2} & -\frac{\sqrt{2} e^{-i\delta/2} \delta m_{21}^2 \tan \theta_{13}}{3\delta m_{32}^2 \cos \theta_{13}} \\ \frac{(2\delta m_{21}^2 + 3\delta m_{32}^2) \sin 2\theta_{13}}{12V_e E} & \frac{\sqrt{2} \delta m_{21}^2 \tan \theta_{13}}{3\delta m_{32}^2 \cos \theta_{13}} & 1 \end{pmatrix}, \quad (\text{A10})$$

which is valid to linear order in both  $\delta m_{32}^2/V_e E$  and  $\delta m_{21}^2/\delta m_{32}^2$ . First-order terms in  $\delta\theta_{12}$  are absent. This again arises because the  $\delta\theta_{12}$  contributions in Eq. (A5) suffer from an additional suppression relative to the leading-order terms in  $\delta\tilde{H}$ . As pointed out in Sec. IIB, the results for antineutrinos can be obtained by reversing the signs of  $V_e$  and  $\delta$  in the above equations.

Note that in  $\tilde{U}_m$  and thus in  $\underline{U}_m$ , corrections containing  $\theta_{13}$  or  $\delta$  are also suppressed by  $\delta m_{21}^2/\delta m_{32}^2 \ll 1$  or  $\delta m_{jk}^2/V_e(0)E \ll 1$ . This implies that for GeV neutrinos at the solar core, the matter mixing is largely unaffected by  $\theta_{13}$  and  $\delta$  perturbations about the tribimaximal case. Significant  $\theta_{13}$  and  $\delta$  effects on the terrestrial fluxes can

therefore only arise through the non-adiabatic transitions described by the matrix  $P$  and through the vacuum mixing matrix  $U$ , which determines the flavor content of the mass states at the detector.

We remind the reader that each column vector in  $\tilde{U}_m$  is only defined up to a phase, an ambiguity without physical significance. The column-vector order in  $\tilde{U}_m$ , on the other hand, is to be selected such that the diagonal elements of  $\tilde{U}_m^\dagger \tilde{H} \tilde{U}_m$  exhibit the same ordering as those of the matrix  $\tilde{M}$ . The arbitrary ordering choice in Eq. (A10) gives

$$\tilde{U}_m^\dagger \tilde{H} \tilde{U}_m = \frac{1}{2E} \begin{pmatrix} 2V_e E + \delta m_{32}^2 \sin^2 \theta_{13} & 0 & 0 \\ 0 & 0 & 0 \\ 0 & 0 & \delta m_{32}^2 \cos^2 \theta_{13} \end{pmatrix} + \dots, \quad (\text{A11})$$

where the ellipsis indicates terms of second or higher order in  $\delta m_{32}^2/V_e E$  and  $\delta m_{21}^2/\delta m_{32}^2$ . The present range of parameters yields  $0 \ll |3 \cos^2 \theta_{13} \delta m_{32}^2| \ll |6V_e E|$ , where the first inequality rests on our assumption that  $\theta_{13}$  is not too large. The correct ordering therefore depends on the signs of  $V_e$  and  $\delta m_{32}^2$ . It follows that the required adjustments can only be implemented once particle type

( $\nu$  vs.  $\bar{\nu}$ ) and mass hierarchy are specified.

Apart from the column-vector order in  $\tilde{U}_m$ , Eq. (A2) can be used to find explicit first-order expressions for  $U_m$ , and thus  $\underline{U}_m$ . The matrix  $\underline{U}_m$  takes the relatively simple form

$$\underline{U}_m = \begin{pmatrix} 1 & 0 & 0 \\ 0 & \cos^2 \theta_{23} & \sin^2 \theta_{23} \\ 0 & \sin^2 \theta_{23} & \cos^2 \theta_{23} \end{pmatrix} + \frac{\sqrt{2} \cos \delta \sin \theta_{13} \sin 2\theta_{23}}{3 \cos^2 \theta_{13}} \begin{pmatrix} 0 & 0 & 0 \\ 0 & 1 & -1 \\ 0 & -1 & 1 \end{pmatrix} \frac{\delta m_{21}^2}{\delta m_{32}^2}. \quad (\text{A12})$$

This expression does not contain  $\mathcal{O}(\delta m_{jk}^2/V_e E)$  and  $\mathcal{O}(\delta\theta_{12})$  terms. Only the sign of  $V_e$  will eventually play a role, as it matters for the column-vector ordering in  $\underline{U}_m$ . It is again apparent that the effects of  $\theta_{13}$  and  $\delta$  on the matrix  $\underline{U}_m$  are suppressed by more than an order of magnitude from the  $\delta m_{21}^2/\delta m_{32}^2$  ratio. For the observable T-conserving matrix elements of  $\underline{U}_m$ , the  $\delta$  depen-

dence can only enter in the combination  $\Re(e^{i\delta} \sin \theta_{13}) = \cos \delta \sin \theta_{13}$ .

## APPENDIX B: EQUALITY OF LOW- AND HIGH-ENERGY FLAVOR RATIOS FOR $\theta_{13} = 0$

In the low-energy limit  $E \rightarrow 0$ , matter effects are negligible, so that  $P \underline{U}_m^T \rightarrow \underline{U}^T$  in Eq. (44). In other words, the vacuum case (18) arises. This general result must hold for all values of the  $\theta_{13}$  angle. In the high-energy limit  $E \rightarrow \infty$ , both  $P$  and  $\underline{U}_m$  in Eq. (44) are nontrivial because all matter effects must be taken into account. It follows that the low- and high-energy limits are distinguished by the difference in the  $\underline{U}^T$  and  $P \underline{U}_m^T$  matrices, where the latter is to be evaluated for neutrinos (as opposed to antineutrinos) in the limit  $E \rightarrow \infty$ . We will show that  $\underline{U}^T$  and  $P \underline{U}_m^T$  are identical when  $\theta_{13} = 0$ .

For  $\theta_{13} = 0$ , the Hamiltonian can be transformed into the form  $H'_F$  given by Eq. (24). As noted in the discussion leading to Eq. (29), the off-diagonal pieces of  $H'_F$  vanish when  $E$  is taken to approach infinity. It follows that  $U_m = R_{23}(\theta_{23})$  is one possible matrix that diagonalizes the original Hamiltonian  $H_F$  at high energies. The remaining ambiguity (up to phases) in the construction of  $U_m$  is determined with our column-vector ordering convention. To this end, we need to fix the mass hierarchy and take  $\delta m_{32}^2 > 0$  as an example. The reader is invited to verify that the inverted hierarchy produces the same final result, as expected due to the decoupling of the  $|3, r\rangle$  state for  $\theta_{13} = 0$ . Note that  $V_e(0)$  is positive because we are considering neutrinos, and not antineutrinos. It follows that the largest eigenvalue in  $H'_F$  is given by  $V_e(0)$  located in the upper left entry. To match our convention, this eigenvalue should appear as bottom right matrix element; the remaining two eigenvalues are already in the correct order. We thus modify our  $U_m$  above with an appropriate permutation matrix, to get

$$U_m = R_{23}(\theta_{23}) \begin{pmatrix} 0 & 0 & 1 \\ 1 & 0 & 0 \\ 0 & 1 & 0 \end{pmatrix} \quad (\text{B1})$$

as the transformation that diagonalizes the high-energy flavor-basis Hamiltonian for  $\theta_{13} = 0$ .

Next, we turn to the crossing-probability matrix  $P$ . For  $E \gg \tilde{E}_{NA}$ ,  $P_c^l \rightarrow \cos^2 \theta_{12}$  and  $P_c^h \rightarrow \cos^2 \theta_{13} = 1$  at the respective lower and higher resonances. Note that the latter of these probabilities is consistent with the fact that the  $|3, r\rangle$  state decouples for  $\theta_{13} = 0$ . Employing these results in Eq. (55) leads to

$$P = \begin{pmatrix} \sin^2 \theta_{12} & \cos^2 \theta_{12} & 0 \\ \cos^2 \theta_{12} & \sin^2 \theta_{12} & 0 \\ 0 & 0 & 1 \end{pmatrix} \begin{pmatrix} 1 & 0 & 0 \\ 0 & 0 & 1 \\ 0 & 1 & 0 \end{pmatrix} \quad (\text{B2})$$

for the crossing probabilities at high energies in the case of a vanishing  $\theta_{13}$  angle.

We are now in the position to give the simple expression

$$P \underline{U}_m^T = \begin{pmatrix} \cos^2 \theta_{12} & \sin^2 \theta_{12} \cos^2 \theta_{23} & \sin^2 \theta_{12} \sin^2 \theta_{23} \\ \sin^2 \theta_{12} & \cos^2 \theta_{12} \cos^2 \theta_{23} & \cos^2 \theta_{12} \sin^2 \theta_{23} \\ 0 & \sin^2 \theta_{23} & \cos^2 \theta_{23} \end{pmatrix} \quad (\text{B3})$$

for the high-energy limit of the matrix  $P \underline{U}_m^T$  for neutrinos. Comparison of this result with  $\underline{U}^T$  then establishes that these two matrices are identical. Therefore, the low- and high-energy terrestrial neutrino flavor ratios are also identical. Moreover, the low-energy antineutrino fluxes, which are obtained by replacing  $U \rightarrow U^*$  in Eq. (17), are equal to the above low-energy neutrino results. Both of these features are apparent in Fig. 2.

## APPENDIX C: PROOF OF FEATURE (i) OF SEC. II C 6

We first note that the level-crossing probabilities presented in Sec. II C 2 act on mass eigenstates, and so are independent of  $\delta$ . It follows that  $\delta$  can only affect the terrestrial neutrino fluxes via the  $\underline{U}$  and  $\underline{U}_m$  flavor-content matrices. This implies that possible phase effects may enter only at the production and detection sites. That neutrino propagation including non-adiabatic transitions in the Sun are unaffected by  $\delta$  does not come as a surprise, as our jump-probability approximation involves only two levels at each resonance, and in two-flavor systems the phase in the mixing matrix can be removed.

Thus, to show that the replacement  $\delta \rightarrow \pi - \delta$  leaves unaffected the  $\nu_e$  and  $\bar{\nu}_e$  spectra, while interchanging the  $\nu_\mu$  and  $\nu_\tau$  spectra, and  $\bar{\nu}_\mu$  and  $\bar{\nu}_\tau$  spectra, it is sufficient to show that the replacement leaves unaffected the first row in both  $\underline{U}$  and  $\underline{U}_m$ , but interchanges the lower two rows. In mathematical terms, we must show that

$$\begin{aligned} (\underline{U})_{ej}(\delta) &= (\underline{U})_{ej}(\pi - \delta), \\ (\underline{U})_{\mu j}(\delta) &= (\underline{U})_{\tau j}(\pi - \delta), \end{aligned} \quad (\text{C1})$$

and

$$\begin{aligned} (\underline{U}_m)_{ej}(\delta) &= (\underline{U}_m)_{ej}(\pi - \delta), \\ (\underline{U}_m)_{\mu j}(\delta) &= (\underline{U}_m)_{\tau j}(\pi - \delta), \end{aligned} \quad (\text{C2})$$

for  $j = 1, 2, 3$ .

Explicit evaluation of  $U(\delta)$  and  $U(\pi - \delta)$  with  $\theta_{32} = 45^\circ$  and  $\theta_{21}$  and  $\theta_{13}$  arbitrary yields

$$\begin{aligned} U_{ej}(\delta) &= U_{ej}(\pi - \delta) & j = 1, 2, \\ U_{ej}(\delta) &= -U_{ej}^*(\pi - \delta) & j = 3, \\ U_{\mu j}(\delta) &= -U_{\tau j}^*(\pi - \delta) & j = 1, 2, \\ U_{\mu j}(\delta) &= U_{\tau j}(\pi - \delta) & j = 3. \end{aligned} \quad (\text{C3})$$

These relations imply our condition (C1), as can be verified by multiplying each equation with its complex conjugate. We remark that this result already establishes Feature (i) for cases with negligible matter effects, such as in vacuum.

Large matter potentials  $V_e(r)$  can definitely modify neutrino flavor fluxes, as we have seen in the text. However, the  $\nu_\mu - \nu_\tau$  relationship is left unaffected by  $V_e(r)$  because only  $\nu_e$  interacts with the solar background electrons. The  $\nu_\mu - \nu_\tau$  part of the above vacuum result,

namely that the  $\nu_\mu$  and  $\nu_\tau$  fluxes switch under  $\delta \rightarrow \pi - \delta$ , should therefore generalize to situations with matter.

To see this explicitly and to establish furthermore that the  $\nu_e$  flux remains unchanged, we need to prove condition (C2). The mixing matrix in matter is defined via Eq. (A1). With the  $\delta$  dependence displayed, this definition reads for  $U_m(\delta)$ :

$$H_M(\delta) = U_m(\delta)^\dagger \left[ U(\delta) \hat{M} U^\dagger(\delta) + \hat{V} \right] U_m(\delta). \quad (\text{C4})$$

In order to relate  $U_m(\pi - \delta)$  and  $U_m(\delta)$ , we start from the analogous equation for  $U_m(\pi - \delta)$ , i.e.,  $H_M(\pi - \delta) = U_m^\dagger(\pi - \delta) \left[ U(\pi - \delta) \hat{M} U^\dagger(\pi - \delta) + \hat{V} \right] U_m(\pi - \delta)$ , and implement the symmetries (C3). In matrix form, these symmetries may be rewritten as

$$U(\pi - \delta) = F U^*(\delta) S, \quad (\text{C5})$$

where the matrix  $F$  interchanges the  $\mu$  and  $\tau$  flavors, and the matrices  $S$  and  $F$  change various signs:

$$F = \begin{pmatrix} -1 & 0 & 0 \\ 0 & 0 & 1 \\ 0 & 1 & 0 \end{pmatrix}, \quad S = \begin{pmatrix} -1 & 0 & 0 \\ 0 & -1 & 0 \\ 0 & 0 & 1 \end{pmatrix}. \quad (\text{C6})$$

The specific expressions for the matrices  $\hat{M}$ ,  $\hat{V}$ ,  $F$ , and  $S$  are such that  $S \hat{M} S^\dagger = \hat{M}$  and  $F \hat{V} F^\dagger = \hat{V}$ . With these observations, the defining relation for  $U_m(\pi - \delta)$  can be cast into the following form:  $H_M(\pi - \delta) = U_m^\dagger(\pi - \delta) F \left[ U^*(\delta) \hat{M} U^T(\delta) + \hat{V} \right] F^\dagger U_m(\pi - \delta)$ . Recalling that  $H_M(\pi - \delta)$ ,  $\hat{M}$ ,  $\hat{V}$ , and  $F = F^\dagger$  are real, complex conjugation of this equation yields:

$$H_M(\pi - \delta) = U_m^T(\pi - \delta) F \left[ U(\delta) \hat{M} U^\dagger(\delta) + \hat{V} \right] F^\dagger U_m^*(\pi - \delta). \quad (\text{C7})$$

By definition, both  $H_M(\pi - \delta)$  and  $H_M(\delta)$  are diagonal. Moreover, they exhibit the same ordering of eigenvalues because they are associated with the same mass hierarchy and particle type ( $\nu$  vs.  $\bar{\nu}$ ). Note also that  $F^\dagger U_m^*(\pi - \delta)$  is unitary. These facts and comparison of Eq. (C7) with Eq. (C4) show that  $F^\dagger U_m^*(\pi - \delta)$  satisfies the defining relation (C4) for  $U_m(\delta)$ . We thus find

$$U_m(\delta) = \begin{pmatrix} e^{i\alpha} & 0 & 0 \\ 0 & e^{i\beta} & 0 \\ 0 & 0 & e^{i\gamma} \end{pmatrix} F^\dagger U_m^*(\pi - \delta). \quad (\text{C8})$$

Here, the three undetermined phases  $\alpha$ ,  $\beta$ , and  $\gamma$  are unobservable, but are included for completeness. The condition (C2) follows now directly from (C8). Feature (i) is thereby established.

## APPENDIX D: PROOF OF FEATURE (ii) OF SEC. II C 6

The general terrestrial flavor fluxes are given by Eq. (44). The matrix  $A \equiv \underline{U} P \underline{U}_m^T$  in this equation can explicitly be obtained at first order with the result (A12). At leading order in the three small parameters  $\delta m_{21}^2/\delta m_{32}^2$ ,  $\delta\theta_{12}$ , and  $\delta\theta_{23}$ , the generic form of  $A$  is

$$A = A_0 + A_m \frac{\delta m_{21}^2}{\delta m_{32}^2} + A_{12} \delta\theta_{12} + A_{23} \delta\theta_{23}. \quad (\text{D1})$$

Here,  $\delta\theta_{12}$  and  $\delta\theta_{23}$  denote deviations from the tribimaximal values of  $\theta_{12}$  and  $\theta_{23}$ , respectively. Note that terms of order  $\delta m_{jk}^2/V_e E$  are absent because they do not enter into  $\underline{U}_m$  in Eq. (A12), and  $U$  in vacuum depends only on the mixing angles. Below we give explicit expressions for the matrices  $A_0$ ,  $A_m$ ,  $A_{12}$ , and  $A_{23}$ . These explicit expressions require the knowledge of the column-vector ordering in Eq. (A12). Thus, the specification of particle type ( $\nu$  vs.  $\bar{\nu}$ ) and the mass hierarchy is necessary.

We seek to prove that in the adiabatic limit ( $P = \mathbb{1}$ ), for NH neutrinos and IH antineutrinos, that  $A_0$  is independent of  $\delta$ ; and that with either mass hierarchy, the first row of  $A_0$  is independent of  $\delta$ . When  $A_0$  is independent of  $\delta$ , then all flavor spectra are independent of  $\delta$  at leading order; when the first row of  $A_0$  is independent of  $\delta$ , then the  $\nu_e$  and  $\bar{\nu}_e$  spectra are independent of  $\delta$  at leading order. Below we determine the full  $\theta_{13}$  and  $\delta$  dependence of  $A_0$ . For completeness, we also determine  $A_{12}$  and  $A_{23}$  at zeroth order in the small parameters. It turns out that  $A_m = 0 + \mathcal{O}(\theta_{13}, \delta\theta_{12}, \delta\theta_{23})$  in all cases, and so we do not consider it any further.

To estimate the effects of non-adiabaticity ( $P \neq \mathbb{1}$ ), we also consider the case of a completely non-adiabatic higher-energy resonance while maintaining adiabaticity at the lower-energy resonance. This requires that  $\theta_{13}$  be small enough such that the non-adiabaticity at the higher-energy resonance occurs at energies where the lower-energy resonance is still adiabatic.

**Neutrinos within the normal hierarchy.** This case is characterized by  $0 < \delta m_{32}^2 < V_e E$ . Inspection of Eq. (A11) shows that the  $\tilde{U}_m$  column vectors in Eq. (A10) need to be rearranged according to  $1 \rightarrow 3 \rightarrow 2 \rightarrow 1$ , i.e.,

$$\tilde{U}_m \rightarrow \tilde{U}_m \begin{pmatrix} 0 & 0 & 1 \\ 1 & 0 & 0 \\ 0 & 1 & 0 \end{pmatrix}. \quad (\text{D2})$$

This gives the following explicit form of the  $A_0$ ,  $A_{12}$ , and  $A_{23}$  matrices:

$$A_0 = \frac{1}{4} \begin{pmatrix} 4s_{13}^2 & 2c_{13}^2 & 2c_{13}^2 \\ 2c_{13}^2 & 1 + s_{13}^2 & 1 + s_{13}^2 \\ 2c_{13}^2 & 1 + s_{13}^2 & 1 + s_{13}^2 \end{pmatrix}, \quad (\text{D3})$$

$$A_{12} = 0, \quad (\text{D4})$$

$$A_{23} = \frac{1}{3} \begin{pmatrix} 0 & -1 & 1 \\ 3 & -1 & -2 \\ -3 & 2 & 1 \end{pmatrix}. \quad (\text{D5})$$

Inspection of Eq. (D3) shows that  $\delta$  leaves unaffected the terrestrial flavor fluxes at leading order, which establishes Feature (ii) for normal-hierarchy neutrinos. Moreover, the second and third rows of  $A_0$  are identical, implying degeneracy between the  $\nu_\mu$  and  $\nu_\tau$  fluxes at this order.

The results (D3), (D4), and (D5) become invalid for

$$A_0 = \frac{1}{6} \begin{pmatrix} 2c_{13}^2 & 2 + s_{13}^2 & 2 + s_{13}^2 \\ 2 + s_{13}^2 - \sqrt{8} c_\delta s_{13} & 2 - \frac{1}{2} s_{13}^2 + \sqrt{2} c_\delta s_{13} & 2 - \frac{1}{2} s_{13}^2 + \sqrt{2} c_\delta s_{13} \\ 2 + s_{13}^2 + \sqrt{8} c_\delta s_{13} & 2 - \frac{1}{2} s_{13}^2 - \sqrt{2} c_\delta s_{13} & 2 - \frac{1}{2} s_{13}^2 - \sqrt{2} c_\delta s_{13} \end{pmatrix}, \quad (\text{D6})$$

$$A_{12} = \frac{1}{3\sqrt{2}} \begin{pmatrix} 4 & -2 & -2 \\ -2 & 1 & 1 \\ -2 & 1 & 1 \end{pmatrix}, \quad (\text{D7})$$

$$A_{23} = \frac{2}{3} \begin{pmatrix} 0 & -1 & 1 \\ -1 & 1 & 0 \\ 1 & 0 & -1 \end{pmatrix}. \quad (\text{D8})$$

In this non-adiabatic case, only the first row of  $A_0$  is independent of  $\delta$ , and so only the  $\nu_e$  and  $\bar{\nu}_e$  spectra are

$$A_0 = \frac{1}{6} \begin{pmatrix} 4c_{13}^2 & 1 + 2s_{13}^2 & 1 + 2s_{13}^2 \\ 3 - 2c_{13}^2 + \sqrt{8} c_\delta s_{13} & \frac{3}{2} + c_{13}^2 - \sqrt{2} c_\delta s_{13} & \frac{3}{2} + c_{13}^2 - \sqrt{2} c_\delta s_{13} \\ 3 - 2c_{13}^2 - \sqrt{8} c_\delta s_{13} & \frac{3}{2} + c_{13}^2 + \sqrt{2} c_\delta s_{13} & \frac{3}{2} + c_{13}^2 + \sqrt{2} c_\delta s_{13} \end{pmatrix}, \quad (\text{D9})$$

$$A_{12} = \frac{1}{3\sqrt{2}} \begin{pmatrix} 4 & -2 & -2 \\ -2 & 1 & 1 \\ -2 & 1 & 1 \end{pmatrix}, \quad (\text{D10})$$

$$A_{23} = \frac{1}{3} \begin{pmatrix} 0 & -1 & 1 \\ -1 & 1 & 0 \\ 1 & 0 & -1 \end{pmatrix}. \quad (\text{D11})$$

Note that there are unsuppressed phase effects, since  $A_0$  depends on  $\delta$ . However, the first row of  $A_0$  remains  $\delta$ -independent.

We remind the reader that resonances are absent in this case. Adiabaticity is therefore ensured trivially, and the results (D9), (D10), and (D11) remain valid in the limit  $\theta_{13} \rightarrow 0$ .

small  $\theta_{13}$ . In this situation, the resonance involving  $|3, r\rangle$  fails to meet the above adiabaticity condition  $P = 1$ : the onset of non-adiabaticity (49) applies here with  $\theta = \theta_{13}$ , which lies below the resonance energy (53) for  $\theta_{13}$  small enough. This non-adiabaticity is associated with the decoupling of the state  $|3, r\rangle$ , as discussed in Sec. II B 1. We display the  $A$ -matrices for a completely adiabatic lower-energy resonance and a completely non-adiabatic higher-energy resonance:

independent of  $\delta$  at lowest order.

**Antineutrinos within the normal hierarchy.** As the sign of  $V_e$  for antineutrinos is opposite that for neutrinos, we have now  $V_e E < 0 < \delta m_{32}^2$ . It follows that the diagonal entries of  $\tilde{U}_m^\dagger \hat{H} \tilde{U}_m$  in Eq. (A11) are correctly ordered already, and adjustments in  $\tilde{U}_m$  are unnecessary. But for antineutrinos we need  $\underline{U}_m^*$  and  $\underline{U}^*$ , which can be obtained by simply changing the sign of  $\delta$  in the final expressions for  $A_0$ ,  $A_{12}$ , and  $A_{23}$ . This yields

**Neutrinos within the inverted hierarchy.** This case is characterized by  $\delta m_{32}^2 < 0 < V_e E$ . Inspection of Eq. (A11) and  $\hat{M}$  establishes that we have to interchange the first and second column in  $\tilde{U}_m$ , which can be implemented via the replacement

$$\tilde{U}_m \rightarrow \tilde{U}_m \begin{pmatrix} 0 & 1 & 0 \\ 1 & 0 & 0 \\ 0 & 0 & 1 \end{pmatrix}. \quad (\text{D12})$$

We then obtain the following expressions for  $A_0$ ,  $A_{12}$ , and  $A_{23}$ :

$$A_0 = \frac{1}{6} \begin{pmatrix} 2 - 2s_{13}^2 & 2 + s_{13}^2 & 2 + s_{13}^2 \\ 2 + s_{13}^2 - \sqrt{8} c_\delta s_{13} & 2 - \frac{1}{2}s_{13}^2 + \sqrt{2} c_\delta s_{13} & 2 - \frac{1}{2}s_{13}^2 + \sqrt{2} c_\delta s_{13} \\ 2 + s_{13}^2 + \sqrt{8} c_\delta s_{13} & 2 - \frac{1}{2}s_{13}^2 - \sqrt{2} c_\delta s_{13} & 2 - \frac{1}{2}s_{13}^2 - \sqrt{2} c_\delta s_{13} \end{pmatrix}, \quad (\text{D13})$$

$$A_{12} = \frac{1}{3\sqrt{2}} \begin{pmatrix} 4 & -2 & -2 \\ -2 & 1 & 1 \\ -2 & 1 & 1 \end{pmatrix}, \quad (\text{D14})$$

$$A_{23} = \frac{2}{3} \begin{pmatrix} 0 & -1 & 1 \\ -1 & 1 & 0 \\ 1 & 0 & -1 \end{pmatrix}. \quad (\text{D15})$$

It is apparent that phase effects are again unsuppressed because  $A_0$  depends on  $\delta$ . However, the first row of  $A_0$  remains  $\delta$ -independent.

Although a resonance is present in the neutrino sector it does not involve the state  $|3, r\rangle$ . Hence, the adiabaticity condition is met, and the results (D13), (D14), and (D15) keep their validity for vanishing  $\theta_{13}$ .

**Antineutrinos within the inverted hierarchy.** In this case, we have  $V_e E < \delta m_{32}^2 < 0$ . Comparison of the eigenvalue ordering in Eq. (A11) with that in  $\hat{M} = \text{diag}(-\delta m_{21}^2, 0, \delta m_{32}^2)/2E$  shows that we have to interchange the first and third column in  $\tilde{U}_m$ , which can be implemented via the replacement

$$\tilde{U}_m \rightarrow \tilde{U}_m \begin{pmatrix} 0 & 0 & 1 \\ 0 & 1 & 0 \\ 1 & 0 & 0 \end{pmatrix}. \quad (\text{D16})$$

The final results for  $A_0$ ,  $A_{12}$ , and  $A_{23}$  are similar to those

for neutrinos within the normal hierarchy:

$$A_0 = \frac{1}{4} \begin{pmatrix} 4s_{13}^2 & 2c_{13}^2 & 2c_{13}^2 \\ 2c_{13}^2 & 1 + s_{13}^2 & 1 + s_{13}^2 \\ 2c_{13}^2 & 1 + s_{13}^2 & 1 + s_{13}^2 \end{pmatrix}, \quad (\text{D17})$$

$$A_{12} = 0, \quad (\text{D18})$$

$$A_{23} = \frac{1}{3} \begin{pmatrix} 0 & 1 & -1 \\ 3 & -2 & -1 \\ -3 & 1 & 2 \end{pmatrix}. \quad (\text{D19})$$

We see that the present  $A_0$  is identical to that in Eq. (D3). It follows that within the adiabatic regime, the net behavior of IH antineutrinos equals that of NH neutrinos within the approximations made in this appendix. Feature (ii) therefore also holds in the present case.

Let us mention an additional aspect shared by NH neutrinos and IH antineutrinos: the presence of the resonance involving  $|3, r\rangle$ . Hence, the results (D17), (D18), and (D19) become invalid for small  $\theta_{13}$ , paralleling the above argument for NH neutrinos. Finally, we quote the result for the completely non-adiabatic limit at the higher-energy resonance:

$$A_0 = \frac{1}{6} \begin{pmatrix} 4c_{13}^2 & 1 + 2s_{13}^2 & 1 + 2s_{13}^2 \\ 3 - 2c_{13}^2 + \sqrt{8} c_\delta s_{13} & \frac{3}{2} + c_{13}^2 - \sqrt{2} c_\delta s_{13} & \frac{3}{2} + c_{13}^2 - \sqrt{2} c_\delta s_{13} \\ 3 - 2c_{13}^2 - \sqrt{8} c_\delta s_{13} & \frac{3}{2} + c_{13}^2 + \sqrt{2} c_\delta s_{13} & \frac{3}{2} + c_{13}^2 + \sqrt{2} c_\delta s_{13} \end{pmatrix}, \quad (\text{D20})$$

$$A_{12} = \frac{1}{3\sqrt{2}} \begin{pmatrix} 4 & -2 & -2 \\ -2 & 1 & 1 \\ -2 & 1 & 1 \end{pmatrix} \quad (\text{D21})$$

$$A_{23} = \frac{1}{3} \begin{pmatrix} 0 & -1 & 1 \\ -1 & 1 & 0 \\ 1 & 0 & -1 \end{pmatrix}. \quad (\text{D22})$$

**Summary** – To summarize this appendix, we have shown that when  $\theta_{32}$  and  $\theta_{21}$  assume their tribimaximal values, then to zeroth order in  $\delta m_{21}^2/\delta m_{32}^2$  and

$\delta m_{32}^2/V_e(0)E$ , one has that

- (i) the  $\nu_e$  and  $\bar{\nu}_e$  spectra are independent of the phase parameter  $\delta$ ;
- (ii) the normal-hierarchy  $\nu_\mu$  and  $\nu_\tau$  spectra are independent of  $\delta$ ; and
- (iii) the inverted-hierarchy  $\bar{\nu}_\mu$  and  $\bar{\nu}_\tau$  spectra are independent of  $\delta$ .

Only the normal-hierarchy  $\bar{\nu}_\mu$  and  $\bar{\nu}_\tau$  spectra, and the inverted-hierarchy  $\nu_\mu$  and  $\nu_\tau$  spectra depend on  $\delta$  in zeroth order. Finally, we remark that the dependence on

$\delta$  in the derived expressions has the form  $\sin\theta_{13}\cos\delta$ , as

required for CP- and T-invariant observables.

- 
- [1] A.G. Riess *et al.* [Supernova Search Team Collaboration], *Astron. J.* **116**, 1009 (1998) [arXiv:astro-ph/9805201]; S.J. Perlmutter *et al.*, [Supernova Cosmology Project Collaboration], *Astrophys. J.* **517**, 565 (1999) [arXiv:astro-ph/9812133]; R.A. Knop *et al.* [Supernova Cosmology Project Collaboration], *Astrophys. J.* **598**, 102 (2003) [arXiv:astro-ph/0309368].
- [2] P. de Bernardis *et al.* [BOOMERanG Collaboration], *Nature* **404**, 955 (2000) [arXiv:astro-ph/0004404]; D.N. Spergel *et al.* [WMAP Collaboration (3 year data)], arXiv:astro-ph/0603449.
- [3] W.J. Percival *et al.* [2dFGRS Collaboration], *Mon. Not. Roy. Astron. Soc.* **327**, 1297 (2001) [arXiv:astro-ph/0105252]; M. Tegmark *et al.* [SDSS Collaboration], *Phys. Rev. D* **69**, 103501 (2004) [arXiv:astro-ph/0310723].
- [4] M. Markevitch *et al.*, *Astrophys. J.* **606**, 819 (2004) [arXiv:astro-ph/0309303].
- [5] K.A. Olive, G. Steigman, and T.P. Walker, *Phys. Rept.* **333**, 389 (2000) [arXiv:astro-ph/9905320]; S. Burles, K.M. Nollett, and M.S. Turner, *Astrophys. J.* **552**, L1 (2001) [arXiv:astro-ph/0010171]; J.M. O'Meara *et al.*, *Astrophys. J.* **552**, 718 (2001) [arXiv:astro-ph/0011179]; R.H. Cyburt, *Phys. Rev. D* **70**, 023505 (2004) [arXiv:astro-ph/0401091].
- [6] For a review of supersymmetric dark matter, see, e.g., G. Jungman, M. Kamionkowski, and K. Griest, *Phys. Rept.* **267**, 195 (1996) [arXiv:hep-ph/9506380].
- [7] J. Lundberg and J. Edsjö, *Phys. Rev. D* **69**, 123505 (2004) [arXiv:astro-ph/0401113], and references therein.
- [8] Another theoretically attractive DM candidate is the axion. In fact, dark matter may consist of more than one species of nonrelativistic particles, possibly accommodating both the LSP and the axion.
- [9] For an overview of particle dark matter and its potential detection, see, e.g., G. Bertone, D. Hooper, and J. Silk, *Phys. Rept.* **405**, 279 (2005) [arXiv:hep-ph/0404175]; F. Halzen and D. Hooper, *Phys. Rev. D* **73**, 123507 (2006) [arXiv:hep-ph/0510048].
- [10] For a review of the potential for dark matter experiments to infer supersymmetry parameters, see, e.g., D. Hooper and A.M. Taylor, *JCAP* **0703**, 017 (2007) [arXiv:hep-ph/0607086].
- [11] W.H. Press and D.N. Spergel, *Astrophys. J.* **296**, 679 (1985); K. Griest and D. Seckel, *Nucl. Phys. B* **283** (1987) 681; A. Gould, *Astrophys. J.* **321**, 571 (1987).
- [12] See, e.g., J. Silk, K.A. Olive, and M. Srednicki, *Phys. Rev. Lett.* **55**, 257 (1985); S. Ritz and D. Seckel, *Nucl. Phys. B* **304**, 877 (1988); R. Gandhi, J.L. Lopez, D.V. Nanopoulos, K. Yuan, and A. Zichichi, *Phys. Rev. D* **49**, 3691 (1994) [arXiv:astro-ph/9309048]; V. Berezhinsky, A. Bottino, J.R. Ellis, N. Fornengo, G. Mignola, and S. Scopel, *Astropart. Phys.* **5**, 333 (1996) [arXiv:hep-ph/9603342]; L. Bergström, J. Edsjö, and P. Gondolo, *Phys. Rev. D* **58**, 103519 (1998) [arXiv:hep-ph/9806293]; J.L. Feng, K.T. Matchev, and F. Wilczek, *Phys. Rev. D* **63**, 045024 (2001) [arXiv:astro-ph/0008115]; V.D. Barger, F. Halzen, D. Hooper, and C. Kao, *Phys. Rev. D* **65**, 075022 (2002) [arXiv:hep-ph/0105182].
- [13] M. Mori *et al.* [KAMIOKANDE Collaboration], *Phys. Rev. D* **48**, 5505 (1993); M. Ambrosio *et al.* [MACRO Collaboration], *Phys. Rev. D* **60**, 082002 (1999) [arXiv:hep-ex/9812020]; M. Ackermann *et al.* [AMANDA Collaboration], *Astropart. Phys.* **24**, 459 (2006) [arXiv:astro-ph/0508518].
- [14] L. Wolfenstein, *Phys. Rev. D* **17**, 2369 (1978); S.P. Mikheyev and A.Yu. Smirnov, *Nuovo Cim. C* **9**, 17 (1986).
- [15] J.R. Ellis, R.A. Flores, and S.S. Masood, *Phys. Lett. B* **294**, 229 (1992).
- [16] A. de Gouvêa, *Phys. Rev. D* **63**, 093003 (2001) [arXiv:hep-ph/0006157].
- [17] P. Crotty, *Phys. Rev. D* **66**, 063504 (2002) [arXiv:hep-ph/0205116].
- [18] M. Cirelli, N. Fornengo, T. Montaruli, I. Sokalski, A. Strumia, and F. Vissani, *Nucl. Phys. B* **727**, 99 (2005) [arXiv:hep-ph/0506298].
- [19] In the process of writing this paper, the present authors became aware of the following advertisement for a Monte Carlo simulation under construction: M. Blennow, J. Edsjö, and T. Ohlsson, *Phys. Scripta* **T127**, 19 (2006).
- [20] P.F. Harrison, D.H. Perkins, and W.G. Scott, *Phys. Lett. B* **530**, 167 (2002) [arXiv:hep-ph/0202074].
- [21] J.F. Beacom, N.F. Bell, D. Hooper, S. Pakvasa, and T.J. Weiler, *Phys. Rev. D* **68**, 093005 (2003) [Erratum-ibid. *D* **72**, 019901 (2005)] [arXiv:hep-ph/0307025].
- [22] A. Bueno, R. Cid, S. Navas-Concha, D. Hooper, and T.J. Weiler, *JCAP* **0501**, 001 (2005) [arXiv:hep-ph/0410206]; O. Mena, S. Palomares-Ruiz, and S. Pascoli, arXiv:0706.3909 [hep-ph].
- [23] J.N. Bahcall, M.H. Pinsonneault, and S. Basu, *Astrophys. J.* **555**, 990 (2001) [arXiv:astro-ph/0010346].
- [24] R. Gandhi, C. Quigg, M.H. Reno, and I. Sarcevic, *Phys. Rev. D* **58**, 093009 (1998) [arXiv:hep-ph/9807264].
- [25] See, e.g., S. Eidelmann *et al.* [Particle Data Group], *Phys. Lett. B* **592**, 1 (2004).
- [26] As collected in F. Plentinger and W. Rodejohann, *Phys. Lett. B* **625**, 264 (2005) [arXiv:hep-ph/0507143].
- [27] The rigorous requirement for  $\nu_\mu$ - $\nu_\tau$  interchange symmetry, slightly more general than the version stated in the text, is that  $\theta_{32}$  be maximal at  $45^\circ$  and that  $\Re(U_{e3})$  vanish.
- [28] To illustrate the physics of adiabatic level permutations, our the column-vector ordering for  $U_m$  has *not* been implemented in Sec. II B 1. In particular, Eq. (29) converts from the flavor to the mass basis at the solar core *without* our convention for  $U_m$ . As a result, the level permutations preceding Eq. (30) have to be implemented by hand.
- [29] See, e.g., T.K. Kuo and J. Pantaleone, *Rev. Mod. Phys.* **61**, 937 (1989).
- [30] S.J. Parke, *Phys. Rev. Lett.* **57**, 1275 (1986).
- [31] H.W. Zaglauer and K.H. Schwarzer, *Z. Phys. C* **40**, 273 (1988).
- [32] Although the phase convention for  $U$  in Ref. [29] differs from ours, these results also hold here: a trivial change of basis relates our leading-order Hamiltonians and theirs,

and the latter serves as the starting point for the Landau–Zener analysis. In other words, this analysis is phase independent because the resonances are treated effectively as two-level systems, so that phases are unobservable.

[33] The results (53) and (54) also maintain their validity with our phase convention. The obvious change of basis to

that in Ref. [29] yields the same leading-order Hamiltonian times phase factors that can be absorbed into the definition of the basis states.

[34] X. Tata, private communication

[35] R. Lehnert and T. J. Weiler, work in progress.